

Alpha kinase 3 signaling at the M-band maintains sarcomere integrity and proteostasis in striated muscle

Received: 20 September 2022

Accepted: 19 January 2023

Published online: 15 February 2023

 Check for updates

James W. McNamara^{1,2,3,4,5}, Benjamin L. Parker^{3,4}, Holly K. Voges^{1,2,6}, Neda R. Mehdiabadi^{1,12}, Francesca Bolk^{1,3}, Feroz Ahmad^{1,2,5}, Jin D. Chung^{1,3,4}, Natalie Charitakis^{1,6}, Jeffrey Molendijk³, Antonia T. L. Zech^{1,2,13}, Sean Lal⁷, Mirana Ramialison^{1,5,6,8}, Kathy Karavendzas^{1,13}, Hayley L. Pointer¹, Petros Syrris^{9,10}, Luis R. Lopes^{9,10}, Perry M. Elliott^{9,10}, Gordon S. Lynch^{3,4}, Richard J. Mills^{1,5,11}, James E. Hudson¹¹, Kevin I. Watt^{1,3,5}, Enzo R. Porrello^{1,2,3,4,5,14}  & David A. Elliott^{1,2,5,6,8,14} 

Muscle contraction is driven by the molecular machinery of the sarcomere. As phosphorylation is a critical regulator of muscle function, the identification of regulatory kinases is important for understanding sarcomere biology. Pathogenic variants in alpha kinase 3 (*ALPK3*) cause cardiomyopathy and musculoskeletal disease, but little is known about this atypical kinase. Here we show that *ALPK3* is an essential component of the M-band of the sarcomere and define the *ALPK3*-dependent phosphoproteome. *ALPK3* deficiency impaired contractility both in human cardiac organoids and in the hearts of mice harboring a pathogenic truncating *Alpk3* variant. *ALPK3*-dependent phosphopeptides were enriched for sarcomeric components of the M-band and the ubiquitin-binding protein sequestosome-1 (*SQSTM1*) (also known as p62). Analysis of the *ALPK3* interactome confirmed binding to M-band proteins including *SQSTM1*. In human pluripotent stem cell-derived cardiomyocytes modeling cardiomyopathic *ALPK3* mutations, sarcomeric organization and M-band localization of *SQSTM1* were abnormal suggesting that this mechanism may underly disease pathogenesis.

Hypertrophic cardiomyopathy (HCM) is defined as the abnormal thickening of the left ventricular wall, affecting an estimated 1 in 200 individuals^{1,2}, making HCM the most common inherited cardiac disorder. Pathogenic variants in genes encoding contractile proteins of the sarcomere are the most prevalent genetic cause of HCM^{2,3}. Critically, maintaining sarcomere integrity relies on quality control mechanisms that identify and remove components damaged under high mechanical and biochemical stress during muscle contraction⁴⁻⁶. The mechanisms by which cardiomyocytes (CMs) maintain sarcomere integrity are poorly understood. A key mechanosensory mechanism

linking the sarcomere to protein quality control pathways is via the kinase domain of the giant sarcomeric protein titin, which recruits the ubiquitin-binding protein p62/sequestosome-1 (*SQSTM1*) to the M-band of the sarcomere^{7,8}. Mutations in the titin kinase domain result in dislocation of *SQSTM1* from the sarcomere into cytosolic aggregates. Very little is known about how sarcomeric signaling cascades at the M-band coordinate protein quality control pathways to maintain sarcomere integrity in striated muscle cells. Although coordinated phosphorylation of sarcomeric proteins has long been recognized as integral to cardiac contractility⁹, few M-band kinases have been

A full list of affiliations appears at the end of the paper. ✉ e-mail: enzo.porrello@mcri.edu.au; David.elliott@mcri.edu.au

identified but include muscle creatine kinase, phosphofructokinase and the titin kinase domain^{7,10–12}. Therefore, defining the sarcomeric kinome and mode of action of kinases is important to provide insights into muscle function and cardiomyopathies.

Multiple genetic studies have linked variants in alpha kinase 3 (*ALPK3*) with HCM^{13–17}. Furthermore, induced pluripotent stem cell (iPSC)-derived CMs from patients homozygous for *ALPK3* loss-of-function variants recapitulate aspects of the HCM phenotype¹⁷ and *Alpk3* knockout mice develop cardiomyopathy¹⁸. *ALPK3* is a member of the atypical alpha kinase family, which have low homology to conventional kinases and are defined by the ability to phosphorylate residues within α -helices¹⁹. In immortalized cell lines, exogenously delivered *ALPK3* localizes to the nucleus²⁰; thus, it has been proposed to regulate transcription factors¹³. Recent stem cell-based modeling of *ALPK3* suggested that *ALPK3* is a sarcomere- and nucleus-localized pseudokinase²¹. However, the kinase domain of *ALPK3* is highly similar to myosin heavy chain kinase, which phosphorylates the tail of myosin heavy chain in *Dictyostelium* to regulate cytoskeletal dynamics²². Given the homology to myosin heavy chain kinase, we hypothesized that *ALPK3* may have a similar role in cytoskeletal signaling in the heart. Clinical data and cellular and animal models all demonstrate that *ALPK3* signaling is critical for cardiac function; therefore, identifying the network of cardiac proteins that rely on *ALPK3* activity may provide insights into the intracellular signaling mechanisms used to control cardiac contractility and, in turn, HCM disease progression, while suggesting new therapeutic targets.

In this study, we addressed the hypothesis that *ALPK3* acts as a cytoskeletal kinase, by using *ALPK3* reporter and mutant human pluripotent stem cell (hPSC) lines, as well as mass spectrometry, to define the role of *ALPK3* in muscle contraction and signaling. Our data demonstrate that *ALPK3* localizes to the M-band of the sarcomere, which is a key regulatory node of sarcomere function⁷. We demonstrate that *ALPK3* is required to maintain a functional contractile apparatus in both hPSC-derived and mouse CMs. Furthermore, phosphoproteomic analysis revealed that *ALPK3* is required to maintain phosphorylation of key sarcomeric proteins. Co-immunoprecipitation (co-IP) experiments showed that *ALPK3* binds to known M-band components such as obscurin (OBSCN). Finally, *ALPK3* phosphorylates and is required for the sarcomeric localization of SQSTM1, an important transporter of polyubiquitinated proteins^{23,24}. These findings suggest that *ALPK3* is an important component of the signaling network that maintains functional sarcomeres.

Results

ALPK3 is a myogenic kinase at the M-band of the sarcomere

To define the expression of *ALPK3* in the human heart, we interrogated a single-nucleus RNA sequencing (snRNA-seq) dataset²⁵ of non-failing adult left ventricle tissue (Fig. 1a). *ALPK3* transcripts were enriched within CMs (fold enrichment approximately 2.43, $P_{\text{adj}} < 10^{-100}$), but also to a lesser extent in smooth muscle cells (fold enrichment approximately 1.21, $P_{\text{adj}} = 6.63 \times 10^{-5}$) (Fig. 1b and Extended Data Fig. 1). To determine the subcellular localization of *ALPK3*, we generated a series of *ALPK3* reporter hPSC lines in which either the tdTomato fluorescent protein or a streptavidin-binding peptide 3 (SBP3)×FLAG tag (SBP3×FLAG) was fused to the C terminus of endogenous *ALPK3* (Extended Data Fig. 2a–c). *ALPK3*-tdTomato was strongly expressed in α -actinin-expressing

hPSC-derived CMs but absent in CD90-expressing stromal cells (Fig. 1c and Extended Data Fig. 2f). Critically, both the *ALPK3*-tdTomato and *ALPK3*-SBP3×FLAG fusion proteins localized to the M-band of the sarcomere (Fig. 1d,e, Extended Data Fig. 2d and Supplementary Video 1) as demonstrated by interdigitiation with Z-disc α -actinin-2 (ACTN2), colocalization with OBSCN and its position between the two A-bands of the sarcomere (MYBPC3). In three-dimensional (3D) reconstructions of live *ALPK3*-tdTomato hPSC CMs, *ALPK3* formed striated patterns consistent with sarcomere localization; no nuclear localization was observed (Supplementary Videos 2 and 3). Moreover, cellular fractionation studies using CMs derived from the *ALPK3*-SBP3×FLAG (Extended Data Fig. 2b–e) line revealed that *ALPK3* was associated with both the myofilament and cytosolic protein fraction (Fig. 1f). The clinical phenotype of *ALPK3* mutations also includes musculoskeletal defects^{13,15,17}. Using a publicly available snRNA-seq dataset for mouse skeletal muscle, we found that *Alpk3* expression in skeletal muscle²⁶ is also restricted largely to myofibers (Extended Data Fig. 2g). In iPSC-derived skeletal muscle cultures, *ALPK3*-tdTomato localized to the M-band, as demonstrated by its localization between Z-disc marker α -actinin (Extended Data Fig. 2h). Together, these results demonstrate that *ALPK3* is restricted to myocytes and probably functions at the sarcomeric M-band in striated muscle. Our finding of *ALPK3* at the contractile apparatus of myocytes challenges the current dogma that *ALPK3* is a nuclear-localized²¹ regulator of transcription factors^{13,20}. These data suggest an alternative hypothesis that *ALPK3* is a regulatory kinase controlling cardiac contraction via phosphorylation of sarcomeric proteins.

Sarcomere organization and calcium handling requires *ALPK3*

To assess the regulatory role of *ALPK3* in CM function, we used an *ALPK3* loss-of-function mutant (*ALPK3*^{C1-60-150delIII}, hereafter *ALPK3*^{mut}) hPSC cell line (Fig. 2a and Extended Data Fig. 3a–c)¹⁷. Cardiac differentiation was unaffected in the *ALPK3*^{mut} line, which produced a similar proportion of hPSC-derived CMs to wild-type (WT) cells, indicated by cardiac troponin T-expressing cells (Extended Data Fig. 3d). These findings suggest that, unlike its paralog *ALPK2* (ref. 27), *ALPK3* is not required for cardiogenesis. *ALPK3*^{mut} CMs displayed disorganization of the sarcomeres and loss of the M-band protein myomesin (MYOM1). We also observed the presence of α -actinin-containing stress fiber-like structures and aggregates (Fig. 2b). Calcium transients in single CMs (Fig. 2c,d) recapitulated patient arrhythmogenicity in *ALPK3*^{mut} hPSC CMs^{13,17} (Fig. 2e). Peak cytosolic calcium levels (Fig. 2f) were elevated while calcium reuptake was delayed in *ALPK3*^{mut} CMs (Fig. 2g). These results demonstrate that *ALPK3*^{mut} hPSC CMs recapitulate key hallmarks of human *ALPK3*-induced cardiomyopathy and suggest that *ALPK3* has a key role in maintaining sarcomere integrity.

ALPK3 deficiency impairs contractility

Human cardiac organoids (hCOs) were generated²⁸ to assess changes in contractile function between WT and *ALPK3*^{mut} heart cells (Fig. 3a,b). Systolic force generation was significantly reduced in *ALPK3*^{mut} hCOs (Fig. 3c) together with a reduction in beating rate (Fig. 3d). Although no changes in contraction or relaxation kinetics were observed (Fig. 3e,f), *ALPK3*^{mut} hCOs were arrhythmogenic (Fig. 3g). Immunofluorescence staining of hCOs for the Z-disc marker ACTN2 and M-band marker OBSCN showed that sarcomeric organization, particularly at

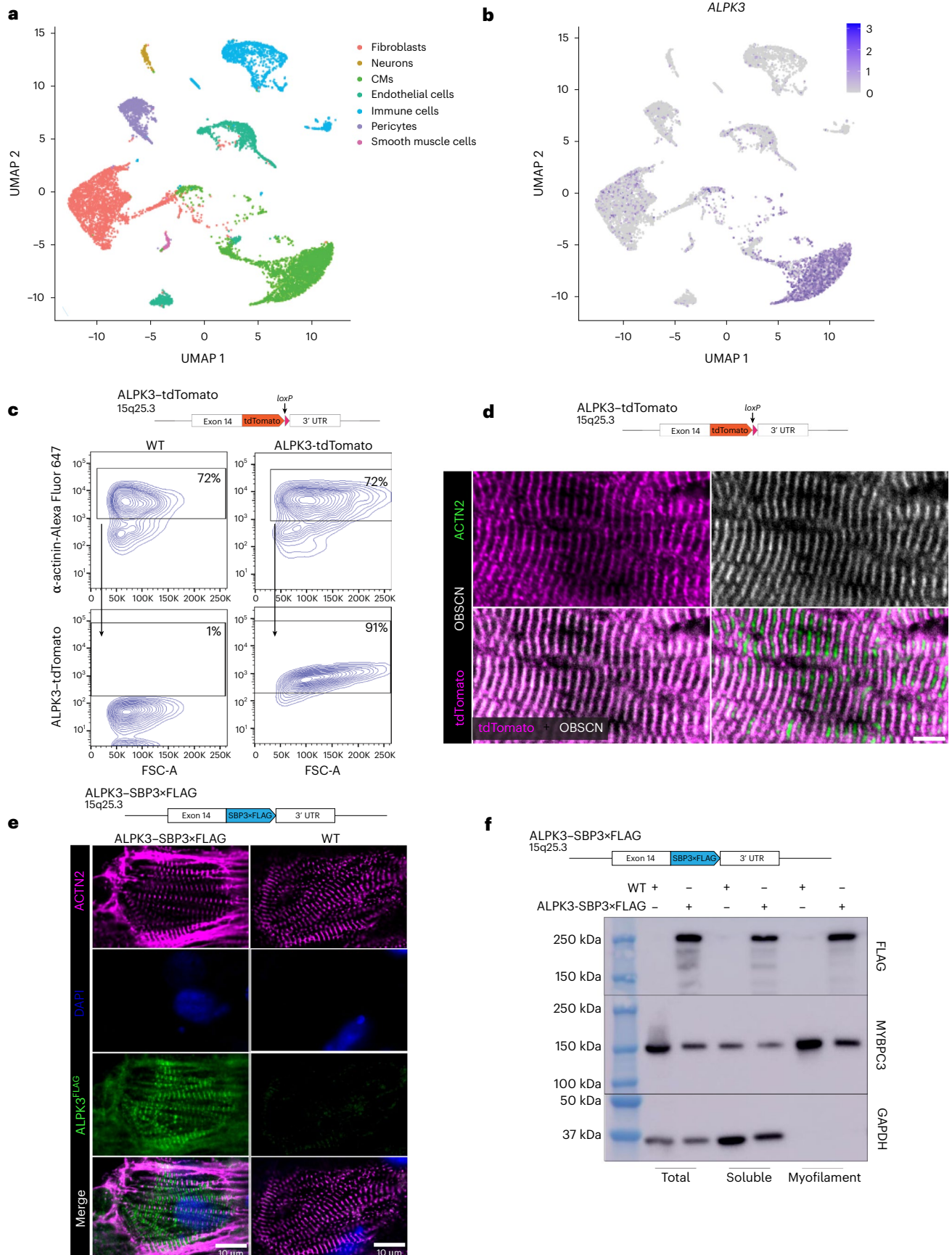
Fig. 1 | *ALPK3* is a myogenic kinase localized to the M-band of the sarcomere.

a, Uniform manifold approximation and projection (UMAP) plot generated from the snRNA-seq of three non-failing adult human hearts. b, Expression pattern of *ALPK3* in cell types of the non-failing adult human heart (colour key shows normalized log(expression) values). c, Schematic of targeting strategy of the *ALPK3*-tdTomato hPSC cell line and flow cytometry of directed cardiac differentiation for α -actinin and *ALPK3*-tdTomato. FSC, forward scatter. d, Representative immunofluorescence microscopy image of nanopatterned

ALPK3-tdTomato hPSC-derived CMs stained for *ALPK3*-tdTomato (green), OBSCN (gray) and α -actinin (magenta); scale bar, 5 μm . e, Schematic of targeting strategy of the *ALPK3*-SBP3×FLAG hPSC cell line and representative immunofluorescence micrograph of WT and *ALPK3*-SBP3×FLAG hPSC CMs stained for α -actinin (magenta), FLAG (green) and DAPI (blue); scale bar, 10 μm . f, Schematic of targeting strategy of *ALPK3*-SBP3×FLAG hPSC cell line and western blot of *ALPK3* in myofilament and cytosolic fractions of CMs.

the M-band, was disrupted in *ALPK3*^{mut} hCOs (Extended Data Fig. 2i). In addition, as observed in two-dimensional myocytes, some aggregation of the M-band component OBSCN and the Z-disc component ACTN2

was apparent in *ALPK3*^{mut} hCOs (Extended Data Fig. 2i). To test our findings that ALPK3 regulates cardiac contractility in vivo, we generated a mouse model containing the variant W1538X (*Alpk3*^{W1538X}), analogous



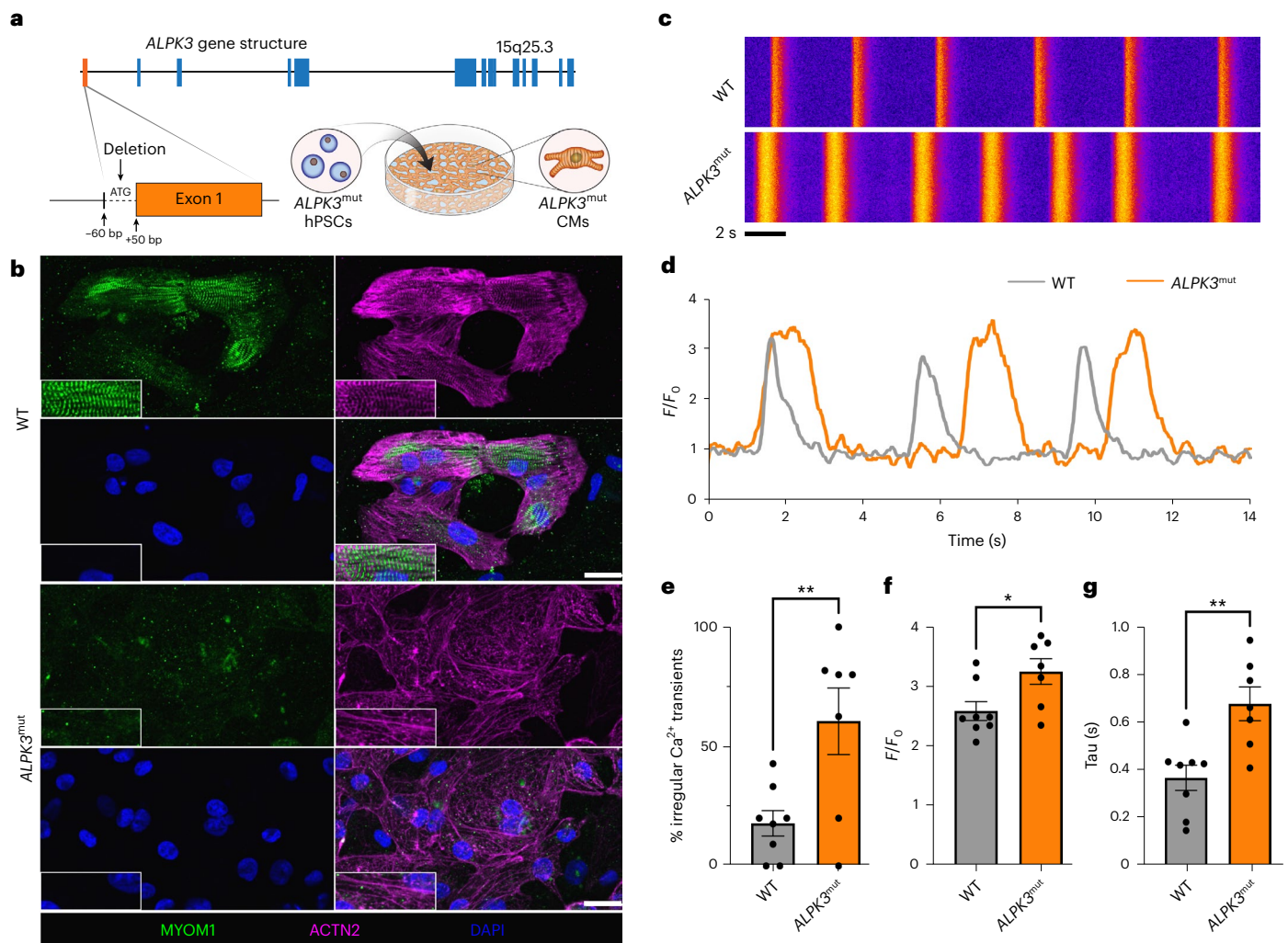


Fig. 2 | ALPK3 is required for sarcomere organization and calcium handling. **a**, *ALPK3* gene structure, schematic of *ALPK3*^{mut} gene targeting and graphic of cardiac differentiation. **b**, Representative immunofluorescence micrograph of WT and *ALPK3*^{mut} hPSC CMs stained for MYOM1 (green), α -actinin (purple) and DAPI (blue); scale bar, 30 μ m. **c**, Representative line scans of Fluo-4 AM calcium handling in WT and *ALPK3*^{mut} hPSC CMs. **d**, Representative calcium transient trace of WT and *ALPK3*^{mut} hPSC CMs. **e**, Percentage of irregular calcium transients

in WT and *ALPK3*^{mut} hPSC CMs. ****** $P = 0.01$. **f**, Peak systolic Fluo-4 AM fluorescence for WT and *ALPK3*^{mut} hPSC CMs. *** $P = 0.026$** . **g**, Time constant (τ) of diastolic calcium reuptake in WT and *ALPK3*^{mut} hPSC CMs. **** $P = 0.003$** . For the calcium handling data (**e–g**), $n = 80$ and 74 cardiomyocytes for WT and *ALPK3*^{mut} over eight and seven independent replicates, respectively. Data are shown as the mean \pm s.e.m. Two-tailed Student's *t*-test.

to the patient-specific variant *ALPK3* c.5294G>A, p.W1765X, causing a truncation in the proximal region of the alpha kinase domain and occurring in a family affected by HCM (Extended Data Fig. 4a,b)¹³. At as early as 3 weeks old, mice homozygous for the variant displayed global enlargement of cardiac chambers by histology (Fig. 3h). Systolic dysfunction and cardiac enlargement were evident by echocardiography at 6 weeks of age (Fig. 3i and Extended Data Fig. 4c). Additionally, transmitral valve Doppler echocardiography showed severe diastolic dysfunction in *Alpk3*^{W538X} mice as indicated by significantly reduced E/A wave ratio and longer isovolumic relaxation times (IVRTs) (Fig. 3i and Extended Data Fig. 4c). Immunofluorescence revealed sarcomeric disarray, particularly at the M-band, as indicated by disorganization of MYOM1 (Extended Data Fig. 4d). Collectively, these results highlight the requirement of ALPK3 to maintain force generation, sarcomere integrity and beating rhythmicity in 3D human cardiac tissue.

ALPK3 deficiency disrupts key cardiac protein networks

To define the ALPK3-dependent molecular networks, we compared the proteomic profiles of purified WT and *ALPK3*^{mut} hPSC CMs (Extended Data Fig. 5a) at days 14 (early) and 30 (late) of cardiac differentiation

(Extended Data Fig. 6). Principal-component analysis demonstrated good reproducibility between replicates, with maturation-dependent changes in the proteomic signature of *ALPK3*^{mut} CMs (Extended Data Fig. 4a). We investigated altered biological processes at days 14 (2,335 differentially expressed proteins; Extended Data Fig. 5b) and 30 (2,106 differentially expressed proteins; Extended Data Fig. 5d). At both time points, pathways related to muscle structure, contraction and stretch-sensing were downregulated in *ALPK3*^{mut} CMs (Extended Data Fig. 5c,e). Furthermore, *ALPK3*^{mut} hPSC CMs exhibited deregulation of pathways related to protein quality control (autophagy, protein ubiquitination, sumoylation) and metabolism (glycolysis, fatty acid oxidation, creatine and ribonucleotide metabolism). Integration of early and late time points showed divergence of many differentially expressed proteins (Extended Data Fig. 5f), demonstrating maturation- or phenotype-dependent shifts in *ALPK3*^{mut} myocytes. Of the 335 proteins commonly upregulated or downregulated at both time points (Extended Data Fig. 5f), pathways that regulate heart development and contraction, sarcomere organization and stretch detection were reduced in *ALPK3*^{mut} CMs (Extended Data Fig. 5g), while cell growth, metabolism, gene expression and microtubule polymerization

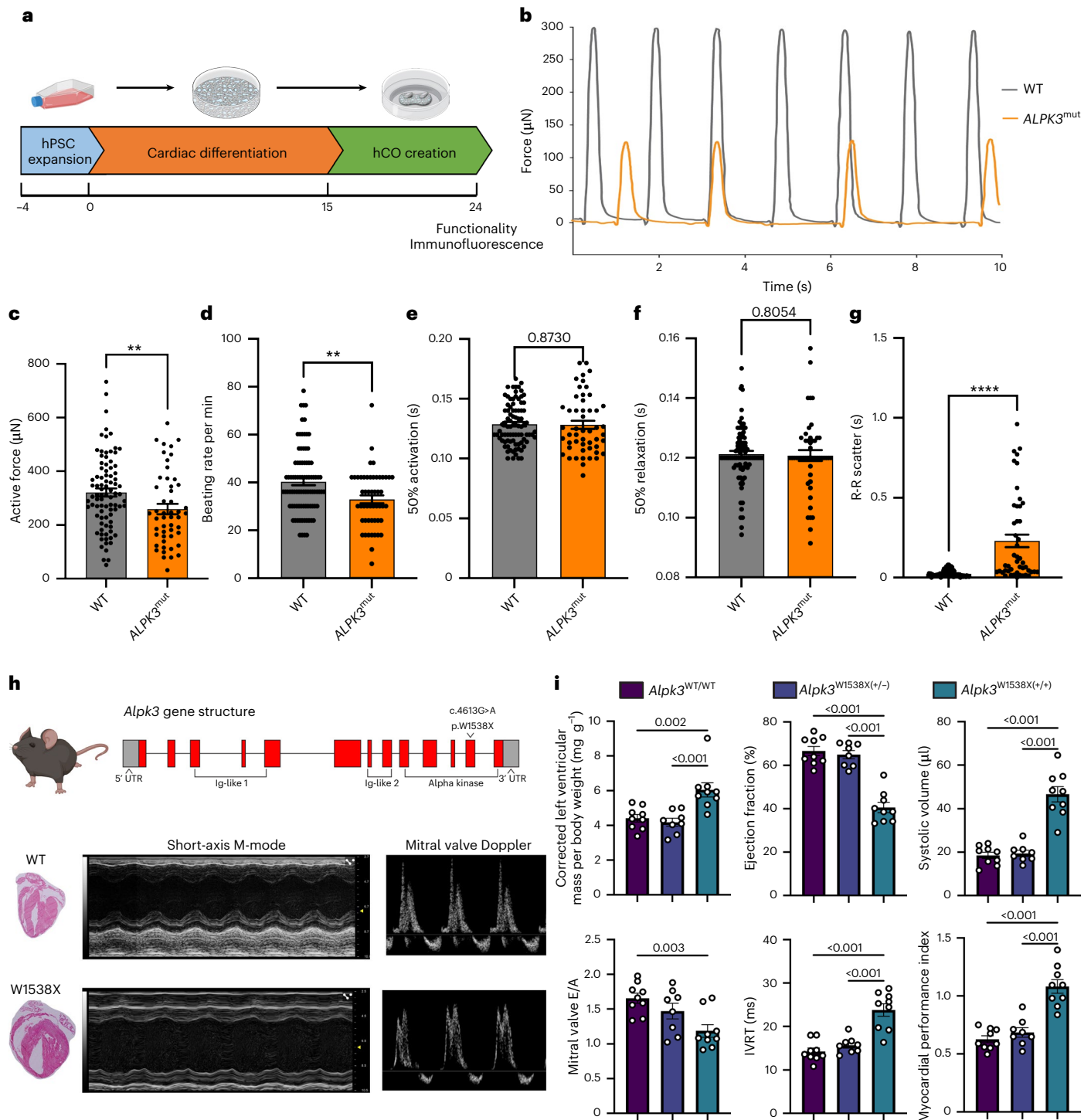


Fig. 3 | ALPK3 deficiency impairs contractility in hCOs. **a**, Experimental outline of the hCO study. **b**, Force traces from representative WT and ALPK3^{mut} hCOs. **c**, Total active force production from WT and ALPK3^{mut} hCOs. ***P* = 0.0073. **d**, WT and ALPK3^{mut} hCO beating rate per minute. ***P* = 0.0049. **e**, Time to 50% activation of WT and ALPK3^{mut} hCOs. **f**, Time to 50% relaxation of WT and ALPK3^{mut} hCOs. **g**, WT and ALPK3^{mut} hCO R-R interval scatter of hCOs to index arrhythmicity. *****P* < 0.0001. **h**, Gene structure of mouse *Alpk3* with location of the W1538X variant, which corresponds to W1765X in humans. Hematoxylin and eosin-stained coronal sections of *Alpk3*^{WT/WT} and *Alpk3*^{W1538X(+/+)} hearts at 21 d and representative M-mode and mitral valve pulse wave Doppler echocardiographs of *Alpk3*^{WT/WT}

and *Alpk3*^{W1538X(+/+)} mice are shown. **i**, Summary echocardiography data of *Alpk3*^{WT/WT}, *Alpk3*^{W1538X(+/-)} and *Alpk3*^{W1538X(+/+)} mice displaying left ventricular mass, ejection fraction, left ventricular systolic volume, E/A wave ratio, IVRT and myocardial performance index. For the hCO experiments, *n* = 82 and 45 hCOs for WT and ALPK3^{mut}, respectively over four independent replicates. Statistical significance was established using a two-tailed Mann–Whitney *U*-test. The error bars represent the s.e.m. For mouse echocardiography, *n* = 9, 8 and 9 mice for *Alpk3*^{WT/WT}, *Alpk3*^{W1538X(+/-)} and *Alpk3*^{W1538X(+/+)}, respectively. Statistical significance was established by ordinary one-way analysis of variance (ANOVA) with Tukey’s multiple-comparisons test. The error bars represent the s.e.m.

pathways were enriched (Extended Data Fig. 5g). These data collectively suggest that ALPK3 contributes to M-band signaling. Importantly, the M-band is understood to be a mechanosensitive regulator of sarcomere organization²⁹, muscle metabolism³⁰ and protein turnover⁸.

Further, RNA-seq analysis revealed that transcriptional differences between WT and *ALPK3*^{mut} hPSC CMs were less pronounced at day 14 than at day 30, suggesting that transcriptional remodeling is secondary to dysregulation of the ALPK3-dependent proteome (Extended Data Fig. 6a,b). RNA-seq data, at both days 14 and 30, identified a suite of commonly downregulated genes in *ALPK3*^{mut} hPSC CMs that were enriched in biological processes related to heart development, contraction and sarcomeric organization (Extended Data Fig. 6c–f). The broad reduction in contractile protein levels was evident, albeit to a lesser extent, in the RNA-seq data (Extended Data Fig. 7). These data suggest that post-transcriptional processes predominantly drive the phenotypic responses in *ALPK3* mutant myocytes.

ALPK3 is critical for the phosphorylation of sarcomeric and protein quality control proteins

To understand potential ALPK3-dependent signaling pathways, we compared the global phosphoproteomic profile of purified WT and *ALPK3*^{mut} CMs, again at two points of differentiation (Fig. 4a). We detected 4,211 phosphorylated peptides with 1,671 and 806 peptides, normalized to total protein abundance, differentially phosphorylated at days 14 and 30, respectively (Fig. 4b,c). At day 14, 1,659 peptides from 526 unique proteins were dephosphorylated in *ALPK3*^{mut} myocytes, which were associated with loss of pathways related to sarcomere assembly, muscle contractility and cell adhesion (Fig. 4d). Autophagy components were dysregulated, suggesting either that this may be a generalized stress response³¹ or that ALPK3 signaling may contribute to the regulation of protein quality control in CMs. Only 12 phosphopeptides from 12 unique proteins were increased in *ALPK3*^{mut} CMs at day 14 (Fig. 4b). Although the number of dephosphorylated peptides was lower at day 30 (1,659 versus 307), the set of 154 unique proteins identified was also enriched in Gene Ontology (GO) terms related to cytoskeletal organization, heart contraction and cell adhesion (Fig. 4e). At the day 30 time point (Fig. 4c), the number of enriched phosphopeptides observed in *ALPK3*^{mut} CMs was dramatically higher than at day 14 (499 versus 12; the 499 peptides represent 271 unique proteins), suggesting that increased phosphorylation is a compensatory signaling response to extended stress with enriched processes including stress response, glycolysis, RNA metabolism and endosome transport (Fig. 4e).

There were 103 peptides from 58 unique proteins that were significantly dephosphorylated in *ALPK3*^{mut} hPSC CMs at both the early and late time points (Fig. 4f). In agreement with the *ALPK3* cardiomyopathy phenotype^{13,17} and impaired contractility (Figs. 2 and 3), commonly dephosphorylated proteins were enriched in the regulation of the cardiac contraction and cytoskeletal organization pathways (Fig. 4g). Taken together, these data suggest that ALPK3 contributes, either directly or indirectly, to the phospho-regulation of key cytoskeletal proteins to maintain sarcomere organization and function.

To further probe the ALPK3-dependent phosphoproteome, we isolated the recombinant ALPK3 kinase domain for biochemical studies (Extended Data Fig. 9a–c). A global kinase assay was performed in phosphorylation-depleted, day 14 *ALPK3*^{mut} hPSC CMs (Fig. 4h). Before the assay, lysates were treated with an irreversible pan-kinase inhibitor to block endogenous kinase activity^{32,33}. When recombinant ALPK3 kinase was applied to lysates, we identified 500 phosphosites that were significantly elevated compared to controls. Notably, a number of cytoskeletal, contractile or proteostasis proteins exhibited greater phosphorylation when lysates were treated with ALPK3 (Fig. 4i and Extended Data Fig. 9d). Correlation between this global kinase assay and day 14 phosphoproteomics data demonstrated agreement between proteins dephosphorylated in *ALPK3*^{mut} CMs and proteins that could be phosphorylated by recombinant ALPK3 (Extended

Data Fig. 8d). These findings favor the hypothesis that ALPK3 is a myogenic kinase that signals via the sarcomeric M-band.

ALPK3 is required for the sarcomeric localization of SQSTM1

Our phosphoproteomic analyses indicated that ALPK3 deficiency caused dephosphorylation of many proteins associated with sarcomere organization and function as well as protein quality control. To identify the ALPK3 protein network, we performed mass spectrometry on proteins enriched by co-IP with endogenous ALPK3 carrying a three-tandem-repeat FLAG tag (Fig. 5a and Extended Data Fig. 2e). Together with ALPK3, 25 proteins were enriched with endogenously FLAG-tagged ALPK3 hPSC CMs over controls (Fig. 5b). Consistent with ALPK3's intracellular localization (Fig. 1d,e), several known M-band proteins associated with ALPK3, such as OBSCN and obscurin-like protein 1 (OBSL1), demonstrating the fidelity of this co-IP experiment (Fig. 1b,c). In addition to the sarcomeric proteins, ALPK3 interacted with proteostasis proteins such as the E3 ligase MuRF2 (TRIM55) and the ubiquitin-binding protein SQSTM1 (p62). Importantly, several ALPK3-bound proteins also demonstrated reduced phosphopeptide abundance (Fig. 5c and Extended Data Fig. 10b) and have been associated with muscle pathology including OBSCN³⁴, OBSL1 (ref. ³⁵), SQSTM1 (ref. ³⁶) and HUWE1 (ref. ³⁷). As both MuRF2 and SQSTM1 are known to interact with titin kinase at the M-band to regulate mechanosensitive signaling and protein turnover⁸, we further investigated the ALPK3–SQSTM1 interaction. We first validated our finding by performing reverse co-IP and found that ALPK3 immunoprecipitated SQSTM1 in ALPK3–SBP3×FLAG hPSC CMs (Extended Data Fig. 9f). We then tested the interaction using a heterologous, nonmuscle system that confirmed the association between ALPK3 and SQSTM1 when these proteins were overexpressed in HEK 293 cells (Fig. 5d). Furthermore, ALPK3 and SQSTM1 colocalized at the M-band of hPSC CMs (Fig. 5e). While total SQSTM1 levels were unchanged between WT and *ALPK3*^{mut} cultures (Fig. 5f), ALPK3 demonstrated the capacity to phosphorylate SQSTM1 (Extended Data Fig. 9d,e) and SQSTM1 was dislocated from the sarcomere and was localized to cytosolic aggregates in *ALPK3*^{mut} hPSC-derived cardiac and skeletal muscle cells (Fig. 5g and Extended Data Fig. 10). To determine whether M-band organization and SQSTM1 localization may underlie pathogenesis in *ALPK3*-associated HCM, we generated three additional hPSC lines harboring *ALPK3* variants (L639fs/34, Q1460X, R1792X) from a recently published cohort of patients with HCM¹⁶. On differentiation into CMs, cells expressing each of these *ALPK3* patient-specific variants recapitulated the key pathological features of sarcomere disorganization and loss of M-band MYOM1 (Fig. 5h). Furthermore, SQSTM1 was not detected in the sarcomeres of these patient-specific variant hPSC lines but formed aggregates either within the cytosol or at the cell membrane (Fig. 5i). Finally, the sarcomeric localization of SQSTM1 was compromised in the myocardium from the *Alpk3*^{W1538X} mouse model (Extended Data Fig. 4e). Collectively, these data suggest that the binding of ALPK3 to SQSTM1 is required for M-band localization of SQSTM1 in striated muscle and disruption of the intracellular localization of SQSTM1 may be a prominent mechanism driving ALPK3-related HCM. Thus, ALPK3 is integral to M-band integrity and signaling as illustrated by the disorganization of MYOM1 (Figs. 2b and 5h and Extended Data Fig. 4), OBSCN (Extended Data Fig. 2i) and SQSTM1 (Fig. 5g,h and Extended Data Fig. 4e) in ALPK3-deficient myocytes.

Discussion

Our data show that ALPK3 is a myogenic kinase that localizes to the M-band of sarcomeres in striated muscle. We define the ALPK3-dependent phosphoproteome in hPSC-derived CMs at two stages of differentiation. Among the proteins that require ALPK3 for phosphorylation are components of the sarcomere, the functional unit that generates the force underpinning muscle contraction. In addition, the phosphorylation status of the cellular protein quality control system is also disrupted in ALPK3-mutant CMs. In this context, we identify that SQSTM1

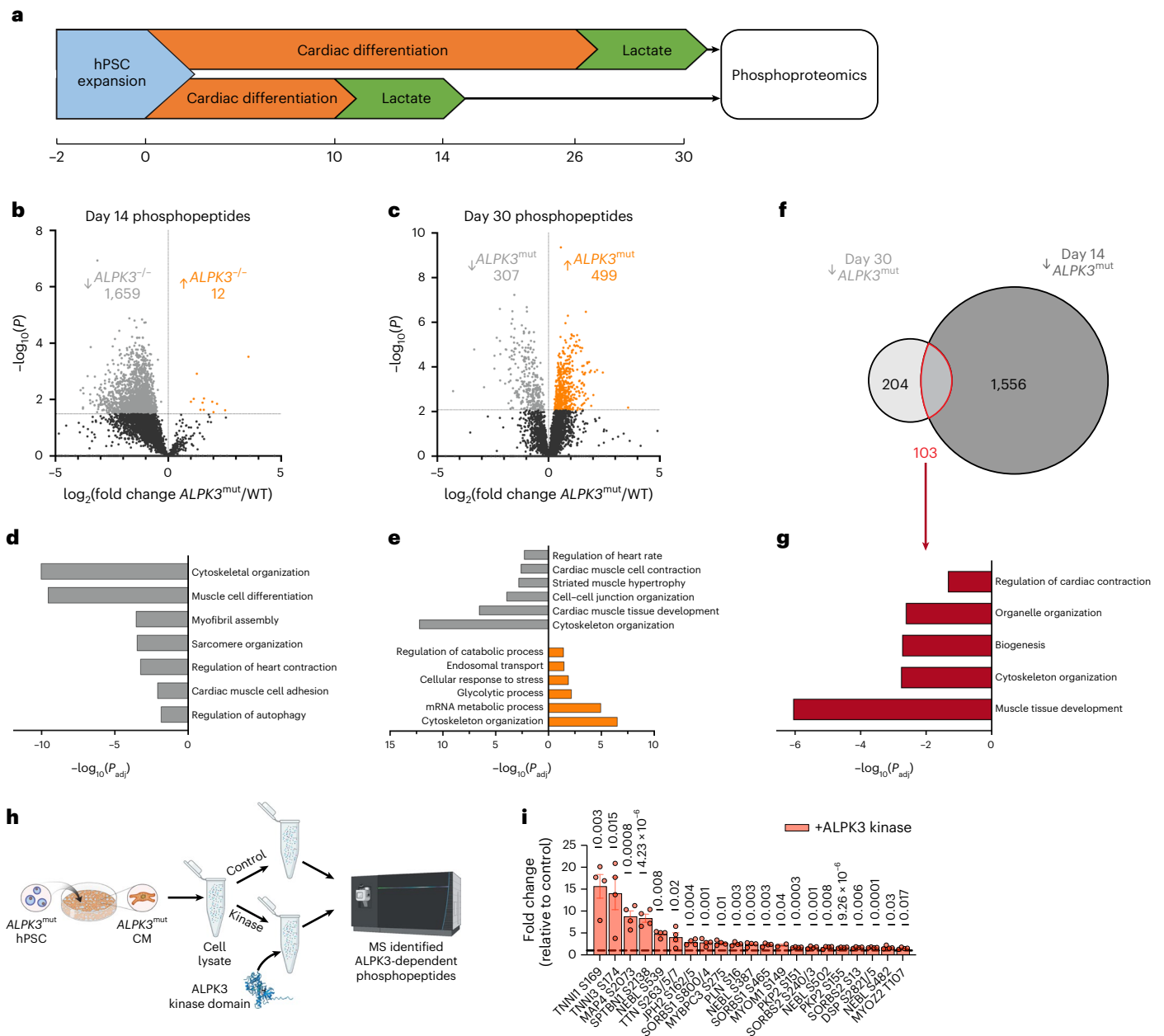


Fig. 4 | ALPK3 is critical for phosphorylation of sarcomeric and autophagy components. **a**, Experimental outline of the phosphoproteomic experiments; $n = 5$ independent differentiations per group. **b**, Volcano plot of day 14 WT and $ALPK3^{mut}$ hPSC CMs to show differential abundance of normalized phosphopeptides. **c**, Volcano plot of WT and $ALPK3^{mut}$ hPSC CMs to show the differential abundance of normalized phosphopeptides at day 30. **d**, GO terms of biological processes enriched in differentially phosphorylated proteins between day 14 WT and $ALPK3^{mut}$ hPSC CMs. **e**, GO terms of biological processes enriched in differentially phosphorylated proteins between day 30 WT and

$ALPK3^{mut}$ hPSC CMs. **f**, Venn diagram showing the overlap of dephosphorylated phosphopeptides in $ALPK3^{mut}$ hPSC CMs between day 14 and day 30. **g**, GO terms of biological processes enriched in commonly dephosphorylated proteins in $ALPK3^{mut}$ hPSC CMs between day 14 and day 30. **h**, Schematic of ALPK3 global kinase assay performed in $ALPK3^{mut}$ hPSC CMs. **i**, Cytoskeletal and contractile proteins with elevated phosphopeptide abundance after the ALPK3 kinase assay. $n = 2-4$ per condition. The dashed bar indicates that the control value = 1. Values represent unadjusted P values from a two-sided t -test. Data are shown as the mean \pm s.e.m.

and MuRF2 both interact with ALPK3 and may provide a mechanism whereby the M-band has a key role in detecting and removing damaged proteins from the sarcomere. Furthermore, ALPK3 is necessary for the M-band localization of SQSTM1. In conclusion, these findings support a major role for ALPK3 in striated muscle contraction and the intracellular signaling networks regulating CM contractility.

Altered CM mechanotransduction is a common feature of cardiomyopathy³⁸. While this has been investigated extensively in the context of the Z-disc signaling pathways^{6,39-41}, comparatively little is

understood about the contribution of M-band biology. Our findings suggest that ALPK3 is a component of the sarcomeric M-band (Fig. 6). A recent study supports this localization²¹ but also reported a nuclear localization that we did not observe. This nuclear localization may be highly context-dependent. Notably, previously published localization studies relied on transient overexpression of the protein in nonmuscle cells or hPSC-derived CMs rather than endogenous tagging of the protein used in this study^{20,21}. Further, ALPK3 is critical for M-band integrity as the established M-band marker MYO1 was not detected at

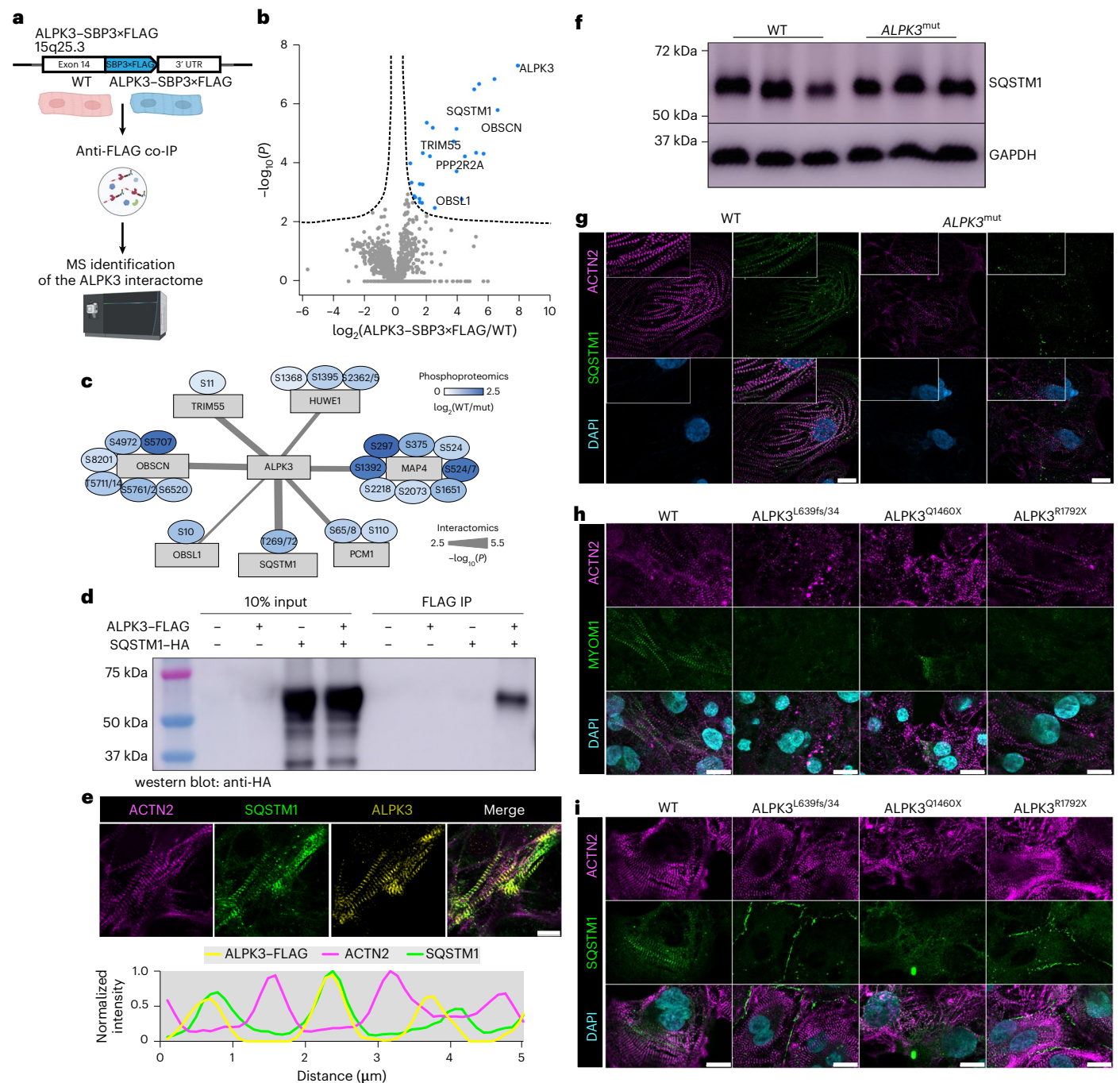


Fig. 5 | ALP3 binds the autophagy regulatory SQSTM1 (p62) and is required for the sarcomeric localization of SQSTM1. **a**, Outline of the co-IP experiment to identify ALP3 interactors. Created with [BioRender.com](https://www.biorender.com). **b**, Volcano plot of enriched peptides in ALP3-SBP3×FLAG hPSC CMs identified by mass spectrometry; $n = 5$ per group. **c**, Network integration of ALP3-bound proteins containing significantly dephosphorylated phosphosites in ALP3^{mut} hPSC CMs. **d**, HEK 293FT co-IP of ALP3-FLAG and SQSTM1-HA. **e**, Immunofluorescence staining of ALP3-FLAG (yellow), SQSTM1 (green) and α -actinin (magenta)

in ALP3-SBP3×FLAG hPSC CMs and intensity plot of all three stains. Scale bar, 15 μm . **f**, Western blot of SQSTM1 levels in WT and ALP3^{mut} hPSC CMs. **g**, Representative immunofluorescence staining of α -actinin (magenta), SQSTM1 (green) and DAPI (blue) in WT and ALP3^{mut} hPSC CMs. Scale bars, 15 μm . **h**, Immunofluorescence staining of MYOM1 (green), α -actinin (magenta) and DAPI (blue) in WT and ALP3 patient-specific variant hPSC CMs. Scale bars, 15 μm . **i**, Immunofluorescence localization of SQSTM1 (green), α -actinin (magenta) and DAPI (blue) in WT and ALP3 patient-specific variant hPSC CMs. Scale bars, 15 μm .

the sarcomere of ALP3-mutant CMs. This loss of M-band MYOM1 was also observed in CMs harboring HCM-associated ALP3 variants and was highly disorganized in a mouse model of ALP3 cardiomyopathy. We propose that ALP3 forms a signaling node at the M-band, which is required to maintain sarcomere integrity. Dysregulation of M-band proteins, including ultrastructural deficits in M-band and thick filament organization, were also observed in a recent independent study²¹.

The titin kinase signalosome is the best understood pathway at the M-band. In this pathway, mechanical stretch induces a conformational change in the kinase domain, which recruits the quality control proteins NBRI, SQSTM1 and MuRF2 to the M-band^{8,42,43}. This pathway regulates cardiac proteostasis in response to mechanical stimuli via MuRF2 regulation of *SRF* gene expression and regulation of SQSTM1 localization⁷. Modeling of ALP3, based on the crystal structure of another alpha

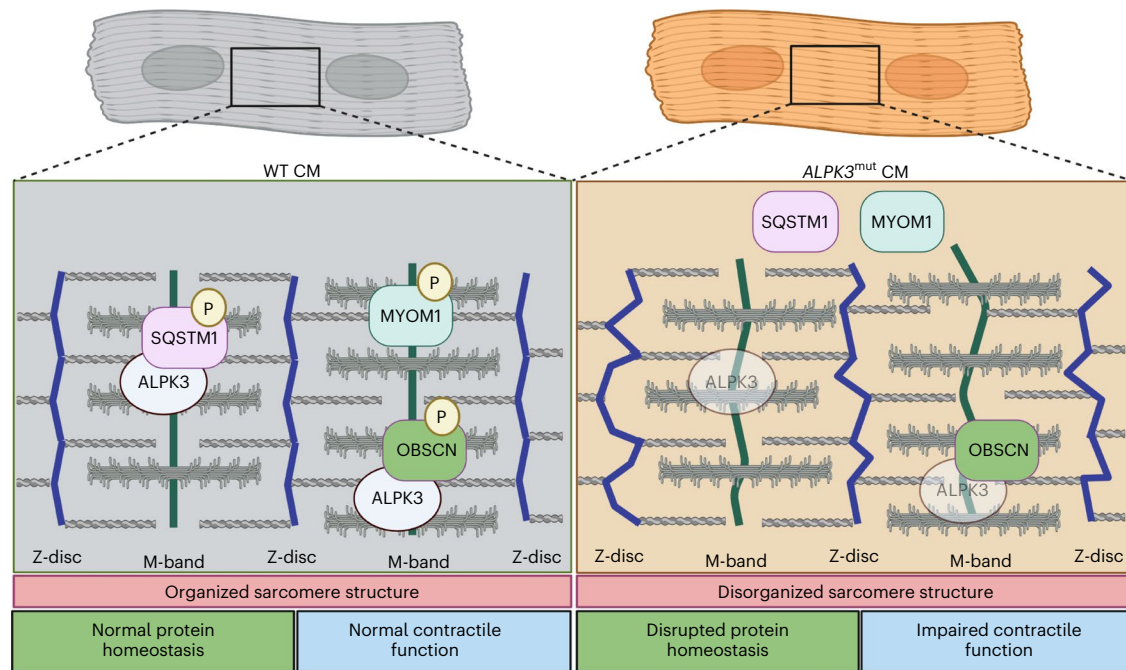


Fig. 6 | Graphical representation of the findings from this study. Graphical summary of key findings from this study of sarcomere disorganization and SQSTM1 and MYOM1 mislocalization in *ALPK3^{mut}* hPSC CMs. Created with [BioRender.com](https://www.biorender.com).

kinase TRPM7, has posited that ALPK3 lacks catalytic activity; thus, it was hypothesized to act as a pseudokinase²¹. In contrast, by means of an unbiased global kinase assay, we found that ALPK3 kinase treatment increased phosphorylation of many proteins, including SQSTM1, which we validated as a direct target. Thus, our study supports the hypothesis that ALPK3 possesses catalytic activity. Future studies including a detailed crystal structure of ALPK3 to define the residues that may regulate catalytic activity are critical. Our data indicate that ALPK3 may form a signaling network with titin kinase, which also binds SQSTM1 and MuRF2 at the M-band, to link mechanical signals to protein quality control networks. For example, the ALPK3–SQSTM1 interaction is required to maintain the sarcomeric localization of SQSTM1, with ALPK3 deficiency leading to mislocalization of SQSTM1 and impaired contractility in hPSC-derived CMs. Additionally, ALPK3 can phosphorylate SQSTM1; this supports the hypothesis that this is mediated through a direct interaction. However, it is possible that this is mediated indirectly. Future studies are required to address the nature of this interaction and its physiological consequences.

Given the longevity of human cardiac muscle cells, efficient protein quality control mechanisms are essential to maintain CM function⁴⁴. The hypertrophic heart experiences sustained biomechanical and oxidative stress. In the myocyte, this translates to increased strain on contractile sarcomere proteins and higher rates of protein misfolding⁴⁵. While this misfolding is initially compensated, protein quality control mechanisms cannot maintain the sustained activity required for normal heart function. Indeed, aberrant protein quality control is a common feature of HCM^{31,45–47}, which eventually leads to compromised cardiac structure and function. In this context, the observation that ALPK3 interacts with regulators of protein homeostasis such as MuRF2 and SQSTM1 within the M-band suggests a role in controlling sarcomeric proteostasis. This model of ALPK3 activity is analogous to that seen for titin kinase at the M-band^{7,12} and BAG3 at the Z-disc⁶, suggesting that sarcomeric integrity is underpinned by the complex interplay between several regulatory pathways. Given our results, which demonstrate mislocalization of SQSTM1 in three independent ALPK3 pathogenic variants, and the growing number of ALPK3 variants linked to HCM^{15,16}, our findings point to a central role

for disrupted sarcomeric homeostasis in cardiomyopathy. Although our findings provide support for a biochemical link between ALPK3 and established regulators of proteostasis (SQSTM1, TRIM55), further studies are required to directly establish whether sarcomeric protein turnover is disrupted due to *ALPK3* mutations.

Our study demonstrates that ALPK3 is required to maintain sarcomere integrity and contractile function in both primary mouse and hPSC-derived CMs. Our findings define ALPK3 as a key functional component of the M-band in striated muscle. In addition, ALPK3 has a role in regulating protein quality control pathways via interactions with SQSTM1 and MuRF2 at the M-band. Given the dysregulation of protein quality control networks in cardiac disease, ALPK3 may be a promising therapeutic target to restore heart function in cardiomyopathies.

Methods

Human ethics statement

All experiments were approved by the Royal Children's Hospital Research Ethics Committee (HREC 33001A). Methods were carried out in accordance with the relevant guidelines and regulations provided by National Health and Medical Research Council (National Statement on Ethical Conduct in Human Research).

Statistics and reproducibility

The investigators were blinded to genotype during the experiments and analysis. No statistical method was used to predetermine sample size. No data were excluded from the analyses. The experiments were not randomized. For confocal microscopy analysis, representative images are shown and experiments were performed a minimum of two times with the experimenter blinded to genotype.

snRNA-seq bioinformatics analysis

snRNA-seq data analysis has been published previously^{25,48}. The bioinformatics analysis pipeline is available at <http://www.heartexplorer.org/> including links retrieved from the analysis website and the source code. Briefly, DoubletFinder (v.2.0.3)⁴⁹ was used to remove doublets. Subsequently, gene filtering discarded mitochondrial and ribosomal genes, as well as genes that were not annotated. Genes that had at

least one count in at least 20 nuclei were retained for further analysis, assuming a minimum cluster size of 20 nuclei. All genes on the X and Y chromosomes were removed before clustering and all subsequent analyses. We performed SCTransform normalization⁵⁰, data integration^{50–52}, data scaling and graph-based clustering separately using the R package Seurat (v.3.0.2). Data integration of the biological replicates for each group was performed using CCA³ from the Seurat package with 30 dimensions and 3,000 integration anchors followed by data scaling. Clustering of the nuclei was performed with 20 principal components and an initial resolution of 0.3. Marker genes to annotate clusters were identified as significantly upregulated genes for each cluster using moderated *t*-tests, accounting for the mean variance trend and employing robust empirical Bayesian shrinkage of the variances, followed by TREAT tests specifying a log fold change threshold of 0.5 and false discovery rate (FDR) cutoff of <0.05, using the R package limma (v.3.40.2).

Stem cell culture and cardiac differentiation

The female HES3 (ref. ⁵³) (WiCell ES03) *NKX2-5^{eGFP/+}* human embryonic stem cell (hESC) line was used for all experiments and has been described previously⁵⁴. The *ALPK3^{mut}* loss-of-function hPSC line was generated previously using CRISPR–Cas9 (ref. ¹⁷). Stem cells were routinely passaged using TrypLE (cat. no. 12604013, Thermo Fisher Scientific) onto Geltrex-coated flasks (cat. no. A1413301, Thermo Fisher Scientific) and mTeSR plus medium (cat. no. 05825, STEMCELL Technologies). The selective ROCK1 inhibitor Y-27632 (cat. no. S6390, Selleck Chemicals) was used when passaging. Differentiation into hPSC CMs was performed using a monolayer culture system with a small-molecule Wnt activation/inhibition protocol²⁵. Briefly, stem cells were plated on day –2 at 20,000 cells per cm² with mTeSR plus (with 10 mM of Y-27632). The next day, the medium was refreshed (without Y-27632). On day 0 of the differentiation, the medium was switched to basal differentiation medium (RPMI 1640 supplemented with 2% B-27 minus vitamin A, 1% GlutaMAX, 1% penicillin-streptomycin) plus 80 ng ml^{–1} Activin A (cat. no. 338-AC, R&D Systems), 8 mM CHIR 99021 (cat. no. 4423, Tocris) and 50 μg ml^{–1} ascorbic acid (cat. no. A5960, Sigma-Aldrich). Twenty-four hours later, the medium was replaced with fresh basal differentiation medium. On day 3, the medium was exchanged to basal differentiation medium containing 5 mM of IWR-1 (cat. no. IO161, Sigma-Aldrich) and 50 μg ml^{–1} of ascorbic acid. Seventy-two hours later, cells were switched back to basal differentiation medium and maintained with medium changes every 48 h. To enrich for myocyte populations, cardiac differentiation was treated for 96 h with glucose-free DMEM containing 5 mM sodium L-lactate, 1% GlutaMAX and 1% penicillin-streptomycin, with medium exchange at 48 h.

Genome editing

Genome editing was performed using CRISPR–Cas9. To generate 3′-tagged ALPK3 cell lines, the guide sequence was cloned into the vector pSpCas9(BB)-2A-eGFP. (The PX458 plasmid was a gift from F. Zhang, cat. no. 48138, Addgene.) Homology-directed repair templates were designed to contain 1,000-bp homology arms flanking the region to be edited. HES3 *NKX2-5^{eGFP/+}* hESCs were nucleofected with the PX458 and repair plasmids. Annealed oligonucleotides were also cloned into the pSpCas9(BB)-2A-eGFP vector for guide RNA sequences in the *ALPK3* patient-specific variant cell lines. Homology-directed repair templates were approximately 80-mer single-stranded oligodeoxynucleotides containing variants plus synonymous variants to prevent recutting by Cas9 of correctly targeted DNA. Details of the sequences used for cell line generation are in the Supplementary Information. HES3 *NKX2-5^{eGFP/+}* hESCs were cotransfected with single-stranded oligodeoxynucleotides and PX458 using Lipofectamine 3000 with the PX458 plasmid. Single green fluorescent protein (GFP)-expressing cells were sorted into 96-well plates and screened by PCR.

Generation of the *Alpk3^{W1538X}* mouse model

The *Alpk3^{W1538X}* mouse model was generated by the MAGEC laboratory (Walter and Eliza Hall Institute) on a C57BL/6J background using CRISPR–Cas9-mediated homology-directed repair. Cas9 mRNA, single-guide RNA and repair template were injected into the cytoplasm of fertilized one-cell-stage embryos generated from WT C57BL/6J breeders. Twenty-four hours later, two-cell-stage embryos were transferred into the uteri of pseudo-pregnant female mice. Viable offspring were genotyped using next-generation sequencing. Details of the sequences used to generate the mouse model are in the Supplementary Information. Mice were fed standard chow and given water ad libitum and were maintained in a 12-h light–12-h dark cycle at ambient room temperature. All experiments were approved by the Animal Ethics Committee of the Murdoch Children’s Research Institute (A949).

Mouse echocardiography

Echocardiography measurements were made on 6- to 8-week-old mice (*n* = 9 (3 males, 6 females), 8 (4 males, 4 females) and 9 (5 males, 4 females) for *Alpk3^{WT/WT}*, *Alpk3^{W1538X(+/-)}* and *Alpk3^{W1538X(+/+)}*, respectively) using a VisualSonics Vevo 3100 ultrasound machine with an MS400 18- to 38-MHz transducer (FujiFilm) under 1–2% isoflurane anesthesia. Cardiac function was reported based on parasternal short-axis M-mode imaging. Diastolic dysfunction was assessed by transmitral pulse wave Doppler flow and tissue annulus Doppler in an apical four-chamber view. All data collection and analysis were performed blinded to genotype.

Mouse histology

Three-week-old mice were anesthetized with 4% isoflurane followed by cervical dislocation. First, mice were perfused transcardially with PBS, which was followed by 4% paraformaldehyde (PFA). Hearts were excised and drop-fixed overnight in 4% PFA. Hearts were sucrose-protected in 15% (v/v) followed by 20% (v/v) sucrose. A scalpel was used to cut hearts into two along the coronal plane and embedded in optimal cutting temperature compound. Then, 10-μm cryosections were cut and stored at –80 °C until staining.

Flow cytometry

Cardiac differentiation was dissociated using 0.25% trypsin EDTA (cat. no. 25200056, Gibco) and filtered into a single-cell suspension. For intracellular flow, cells were fixed in 2% PFA for 10 min before permeabilization with 0.25% Triton X-100. Primary antibody staining used α-actinin (1:100 dilution, cat. nos. A7811 (Sigma-Aldrich) and ab68167 (Abcam)) or cardiac troponin T (1:100 dilution, cat. no. ab8295, Abcam) as CM markers and CD90 (1:100 dilution, cat. no. 328124, BioLegend) as a stromal cell marker. Data were acquired on a BD LSRFortessa X-20 Cell Analyzer and a BD FACSDiva (v.9.0.1) and analyzed using FlowJo (v.10.8.1) software.

Immunofluorescence

Cells were washed with PBS before being fixed with 2% PFA for 30 min at room temperature. Before staining, cells were permeabilized in 0.1% Triton X-100 in PBS for 30 min and blocked in 5% BSA in PBS-Tween 20 (PBS-T) for 1 h. Primary antibodies were incubated overnight at 4 °C. Cells were washed three times for 5 min in PBS-T before incubation with secondary antibodies for 1 h at room temperature. For mouse hearts, cryosections were brought to room temperature and slides underwent antigen retrieval before using the same staining protocol. The complete list of antibodies used for immunofluorescence and dilutions is included in the Reporting summary. Images were analyzed with the Zen Black 2012 (v.2.3 SP1, ZEISS) and ImageJ (v.2.3.0/1.53q, NIH) software.

Sample preparation for global (phospho)proteomics

Samples were washed three times with ice-cold PBS. Cells were then scraped off the dish using 4% (w/v) sodium deoxycholate in 100 mM

Tris-HCl, pH 8.5, before heating at 95 °C for 5 min. Cell lysates were allowed to cool on ice for 5 min before snap-freezing on dry ice and were stored at –80 °C. Samples were thawed on ice, quantified with a bicinchoninic acid (BCA) assay (Thermo Fisher Scientific) and normalized to 300 µg per 200 µl. Protein was reduced to a final concentration of 10 mM Tris(2-carboxyethyl)phosphine hydrochloride (Sigma-Aldrich) and alkylated with 40 mM of 2-chloroacetamide (Sigma-Aldrich) for 5 min at 45 °C. Samples were cooled on ice and then digested with 3 µg of sequencing-grade trypsin (Sigma-Aldrich) and 3 µg of sequencing-grade Lys-C (Wako) overnight at 37 °C. A 5-µg aliquot was removed for total proteomic analysis and the phosphopeptides were enriched from the remaining digest using the EasyPhos protocol as described previously⁵⁵.

Sample preparation for the ALPK3 interactome

Protein G Dynabeads were resuspended in 50 µl of 2 M urea, 50 mM Tris, pH 7.5, containing 1 mM of Tris(2-carboxyethyl)phosphine hydrochloride, 5 mM of 2-chloroacetamide, 0.2 µg of trypsin and 0.2 µg of Lys-C and digested overnight at 37 °C with shaking at 1,800 r.p.m. Peptides were removed, diluted with 150 µl of 1% trifluoroacetic acid (TFA) and desalted on poly(styrenedivinylbenzene) reversed phase support micro-columns (Sigma-Aldrich) as described previously⁵⁵. The columns were washed with 99% isopropanol containing 1% TFA followed by 5% acetonitrile containing 0.2% TFA and then eluted with 80% acetonitrile containing 1% ammonium hydroxide and dried by vacuum centrifugation.

Expression and purification of ALPK3 recombinant kinase

The recombinant kinase domain of ALPK3 was bacterially expressed in One Shot BL21(DE3) *Escherichia coli* (Thermo Fisher Scientific). The DNA sequence encoding amino acids 1577–1828 (IDT) was subcloned into the PET-28a⁺ T7 expression vector sequenced to confirm correct insertion. For large-scale expression, 25 ml of overnight culture was shaken with lysogeny broth containing 50 µg ml⁻¹ kanamycin at 37 °C until an OD₆₀₀ reached approximately 0.8. The culture was then induced with 1 mM of isopropyl-beta-D-thiogalactopyranoside and shaken for approximately 24 h at 20 °C. Pellets were snap-frozen and stored at –80 °C. For purification, cell pellets were thawed and resuspended in *E. coli* lysis buffer (300 mM NaCl, 50 mM NaH₂PO₄, 10 mM imidazole, pH 8.0) with protease inhibitors and sonicated four times for 30 s at 50% with 2-min rests on ice between pulses. Lysates were cleared using centrifugation (3,200 r.p.m. for 15 min at 4 °C) and the clarified lysate was incubated with HisPur Ni-NTA resin (Pierce) to bind histidine-tagged proteins. The resin was then successively washed with wash buffer I (300 mM NaCl, 50 mM NaH₂PO₄, 20 mM imidazole, pH 8.0) and II (300 mM NaCl, 50 mM NaH₂PO₄, 50 mM imidazole, pH 8.0). Ten 1-ml fractions were collected using gravity-based column chromatography using elution buffer (300 mM NaCl, 50 mM NaH₂PO₄, 250 mM imidazole, pH 8.0), which was followed by a second 10-ml bulk. Pure fractions were combined for concentration and buffer exchange using 10 MWCO Protein Concentrators (Pierce).

ALPK3 global kinase assay

Metabolically purified ALPK3^{mut} hPSC CMs were used to identify substrates for ALPK3; 10-cm² dishes of ALPK3^{mut} hPSC CMs were collected in 1 ml of co-IP buffer with cOmplete, EDTA-free protease inhibitor cocktail (Roche) and PhosSTOP phosphatase inhibitor (Roche) and snap-frozen on dry ice. On the day of the assay, lysates were thawed on ice and sheared with ten strokes through a 22-gauge needle followed by three strokes through a 27-gauge needle. To irreversibly inhibit endogenous kinase activity, lysates were treated with 10 mM 5'-(4-fluorosulfonylbenzoyl)adenosine hydrochloride for 30 min at 30 °C with shaking at 1,200 r.p.m. (refs. ^{32,33}). Samples were concentrated and dialyzed extensively to remove 5'-(4-fluorosulfonylbenzoyl)

adenosine hydrochloride using 10 MWCO Protein Concentrators. A BCA assay was run to determine protein concentration. Each sample was split into two 0.75-mg aliquots and the volume was brought to 400 µl with co-IP buffer. An equal volume of 2× kinase assay buffer (50 mM Tris-HCl, pH 7.4, 10 mM MgCl₂, 3 mM MnCl₂, 2 mM dithiothreitol, 0.5 mM ATP) was added to each tube. One tube per sample received either 25 µg of recombinant ALPK3 kinase or an equivalent volume of water. Tubes were incubated at 30 °C for 3 h with shaking at 1,200 r.p.m. All samples were then snap-frozen on dry ice and stored at –80 °C until processing for mass spectrometry (MS)-based identification of phosphopeptides.

Liquid chromatography–tandem MS acquisition

Peptides were resuspended in 2% acetonitrile containing 0.1% TFA and analyzed on a Dionex 3500 nano-HPLC coupled to an Orbitrap Eclipse mass spectrometer (Thermo Fisher Scientific) via electrospray ionization in positive mode with 1.9 kV at 275 °C and radio frequency set to 40%. Separation was achieved on a 50 cm × 75 µm column packed with C18AQ (1.9 µm, Dr. Maisch; PepSep) over 60 min at a flow rate of 300 nl min⁻¹. The peptides were eluted over a linear gradient of 3–40% Buffer B (Buffer A: 0.1% formic acid; Buffer B: 80% v/v acetonitrile, 0.1% v/v formic acid) and the column was maintained at 50 °C. The instrument was operated in data-independent acquisition mode with an MS¹ spectrum acquired over the mass range of 350–950 *m/z* (60,000 resolution, 2.5 × 10⁶ automatic gain control and 50-ms maximum injection time) followed by tandem MS analysis with a higher-energy C-trap dissociation of 37 × 16 *m/z* with 1-*m/z* overlap (28% normalized collision energy, 30,000 resolution, 1 × 10⁶ automatic gain control, automatic injection time).

Liquid chromatography–tandem MS data processing

Data were searched against the UniProt human database (June 2021; UP000000589_109090 and UP000000589_109090_additional) with Spectronaut 15.1.210713.50606 using default parameters with peptide spectral matches, peptide and protein FDR set to 1%. All data were searched with oxidation of methionine set as the variable modification and carbamidomethylation set as the fixed modification. For the analysis of phosphopeptides, phosphorylation of serine, threonine and tyrosine was set as a variable modification. Quantification was performed using MS²-based extracted ion chromatograms using 3–6 fragment ions >450 *m/z* with automated fragment ion interference removal as described previously⁵⁶.

Proteomic and phosphoproteomic statistical and downstream analysis

Data were processed with Perseus⁵⁷ to remove decoy data, potential contaminants and proteins only identified with a single peptide containing oxidized methionine. The 'Expand Site' function was additionally used for phosphoproteomic data to account for multiphosphorylated peptides before statistical analysis. For the phosphoproteomic and proteomic analysis, data were log₂-transformed and normalized by subtracting the median of each sample. Data were filtered to contain phosphosites quantified in at least three biological replicates and statistical analysis was performed with ANOVA, including correction for multiple-hypothesis testing using a Benjamini–Hochberg FDR with *q* < 0.05 defined as a significance cutoff. For the interactome analysis, data were log₂-transformed and normalized by subtracting the median of each sample. Data were filtered to contain proteins quantified in at least three biological replicates of the ALPK3 pull-down group. Analyses with missing data in all the replicates of the negative control group were imputed using random values from a downshifted normalized distribution of the entire dataset. Differentially enriched proteins were calculated using *t*-tests including correction for multiple-hypothesis testing using a Benjamini–Hochberg FDR with *q* < 0.05 defined as a significance cutoff.

RNA isolation

Samples were collected in TRIzol and frozen at -80°C until processing. RNA extraction was performed first by phase separation with chloroform (200 μl per 1 ml of TRIzol) and purified using a column-based procedure (cat. no. 74104, QIAGEN) with DNase I treatment.

RNA-seq and analysis

Paired sequence reads underwent quality trimming using Skewer (v.0.2.2) with default settings⁵⁸. Subsequently, RNA-seq reads were aligned to the human reference genome sequence (hg38) using STAR aligner (v.2.5.3a) with default settings⁵⁹. Annotations and genome files (hg38) were obtained from Ensembl (release 105). Uniquely mapped reads with mapping quality ($Q \geq 30$) were counted across genes with featureCounts (subread 2.0.0)⁶⁰. Using the annotation package org.Hs.eg.db, ribosomal and mitochondrial genes as well as pseudogenes, and genes with no annotation (Entrez Gene ID), were removed before normalization and statistical analysis. In this dataset, only genes with >0.5 counts per million in at least four samples were retained for statistical analysis. Differential gene expression analysis was performed in R (v.3.6.0) with the Bioconductor package edgeR (v.3.36.0)⁶¹ in RStudio. An FDR < 0.05 using the Benjamini–Hochberg correction⁶² was used.

Creation of hCOs

hCOs were created as described previously^{28,63}. Briefly, day 15 cardiac differentiation was dissociated to a single-cell suspension. Acid-solubilized collagen I (Devro) was salt-balanced with $10\times$ DMEM, pH-neutralized with 0.1 M NaOH and mixed sequentially on ice with Matrigel and cells. Each hCO contained 5×10^4 cells in 2.6 mg ml^{-1} collagen I and 9% Matrigel in a volume of 3.5 μl . After gelling for 60 min at 37°C and 5% CO_2 , hCOs were cultured in α -MEM GlutaMAX (Thermo Fisher Scientific), 10% FCS, 200 mM L-ascorbic acid 2-phosphate sesquimagnesium salt hydrate (Sigma-Aldrich) and 1% penicillin-streptomycin (Thermo Fisher Scientific) with the medium changed every 2–3 d. Nine days after hCOs were created, active force production was measured by analyzing hCO pole deflection; 10-s videos were collected at 100 Hz using a Leica Thunder DMI8 inverted microscope. Videos were analyzed to describe contractile parameters using a previously described MATLAB code²⁸.

Calcium imaging

Calcium imaging was performed using Fluo-4 AM (cat. no. F-14201, Invitrogen). Briefly, cells were incubated in Tyrode's buffer (140 mM NaCl, 5.4 mM KCl, 1 mM MgCl_2 , 10 mM glucose, 1.8 mM CaCl_2 , 10 mM HEPES, pH 7.4) containing 5 mM Fluo-4 AM and 0.02% pluronic acid F-127 for 30 min at 37°C . Cells were then washed with Tyrode's buffer for 30 min. Line scans were collected at a frequency of 100 Hz using an LSM900 and $\times 40$ oil objective.

Immunoprecipitation

Lactate-purified CMs were washed with cold PBS before lysis in co-IP buffer (150 mM NaCl, 50 mM Tris-HCl, pH 7.5, 10% glycerol, 0.1% Triton X-100). Lysates were incubated at 4°C with agitation for 1 h. Insoluble matter was pelleted by centrifugation at $12,000g$ for 15 min at 4°C . Each reaction was incubated in 2 μg of anti-FLAG M2 (cat. no. F1804, Sigma-Aldrich) for 2 h at 4°C and incubated with 40 μl washed Dynabeads Protein G (cat. no. 10003D, Invitrogen) for 1 h. Beads were collected using magnetic separation and washed twice in cold lysis buffer followed by three washes in cold PBS. The buffer was aspirated and the beads were snap-frozen on dry ice. For the reverse binding experiments, 2 mg of lysate from metabolically purified ALPK3–SBP3 \times FLAG hPSC CMs was immunoprecipitated for 3 h at 4°C using an anti-SQSTM1 antibody (cat. no. ab56416, Abcam) followed by Dynabeads Protein G for 1 h. Beads were washed with co-IP buffer, resuspended in $1\times$ Laemmli sample buffer and heated at 70°C for 10 min. ALPK3–SBP3 \times FLAG and SQSTM1 were detected by western blot using anti-FLAG M2 (1:1,000 dilution) or anti-SQSTM1 antibody (1:2,000 dilution), respectively.

HEK 293 cell transfection

HEK 293FT cells (cat. no. R70007, Invitrogen) were cultured in $1\times$ DMEM, 10% FCS, 0.1 mM nonessential amino acids (Thermo Fisher Scientific), 1% GlutaMAX, 1% penicillin-streptomycin and 500 mg ml^{-1} geneticin (Gibco). HEK 293FT cells were plated at 625,000 cells per well of a six-well culture plate. Plasmids were transfected using Lipofectamine 3000 in the above medium without antibiotics. After 24 h, medium was changed and refreshed to include antibiotics and cells were collected for downstream applications the next day.

Targeted ALPK3 kinase assay

SQSTM1 containing a C-terminal hemagglutinin (HA) tag was overexpressed in HEK 293FT cells for 72 h using Lipofectamine 3000. Samples were collected in co-IP buffer plus protease inhibitor, snap-frozen on dry ice and stored at -80°C until use. On the day of the experiment, lysates were thawed on ice and sheared with ten strokes through a 22-gauge needle followed by three strokes through a 27-gauge needle. ABCA assay was performed and 2 mg of lysate was immunoprecipitated for 2 h with a 2 μg of an anti-HA antibody (cat. no. ab9110, Abcam) and Dynabeads Protein A (cat. no. 10002D, Invitrogen) for an additional 1 h. Beads were washed in co-IP buffer before being split equally between tubes. Beads were resuspended in 500 μl of kinase assay buffer plus protease inhibitor. One tube received 5 μg active ALPK3 kinase and one received 5 μg of heat-denatured ALPK3 kinase. Tubes were incubated at 30°C for 3 h with shaking at 1,200 r.p.m. On completion, beads were washed with kinase assay buffer and split equally again into two tubes. Half were snap-frozen, while half were treated with lambda protein phosphatase (New England Biolabs) before freezing. Samples were thawed and resuspended in $1\times$ Laemmli sample buffer and heated to 70°C for 10 min. Equal volumes were then run on a 6% acrylamide gel containing 25 μM Phos-tag (Wako Chemicals) to separate phosphorylated species. Blots were transferred to a polyvinylidene fluoride membrane and probed with an anti-phospho-SQSTM1 antibody (T269/S272, 1:1,000 dilution, cat. no. 3121S, Cell Signaling Technology).

Reporting summary

Further information on research design is available in the Nature Portfolio Reporting Summary linked to this article.

Data availability

All proteomics raw data have been deposited in the PRoteomics IDentification Database under accession nos. [PXD035535](#) (total and phosphoproteomics data of WT versus *ALPK3^{mut}*), [PXD035734](#) (ALPK3–SBP3 \times FLAG affinity purification) or [PXD038544](#) (global kinase assay). The RNA-seq data have been deposited in the Gene Expression Omnibus under accession no. [GSE215304](#). Other data and reagents are available upon reasonable request. Source data are provided with this paper.

References

1. McNally, E. M., Barefield, D. Y. & Puckelwartz, M. J. The genetic landscape of cardiomyopathy and its role in heart failure. *Cell Metab.* **21**, 174–182 (2015).
2. Semsarian, C., Ingles, J., Maron, M. S. & Maron, B. J. New perspectives on the prevalence of hypertrophic cardiomyopathy. *J. Am. Coll. Cardiol.* **65**, 1249–1254 (2015).
3. Marian, A. J. & Braunwald, E. Hypertrophic cardiomyopathy: genetics, pathogenesis, clinical manifestations, diagnosis, and therapy. *Circ. Res.* **121**, 749–770 (2017).
4. Cohn, R. et al. A contraction stress model of hypertrophic cardiomyopathy due to sarcomere mutations. *Stem Cell Rep.* **12**, 71–83 (2019).
5. Martin, T. G. & Kirk, J. A. Under construction: the dynamic assembly, maintenance, and degradation of the cardiac sarcomere. *J. Mol. Cell. Cardiol.* **148**, 89–102 (2020).

6. Martin, T. G. et al. Cardiomyocyte contractile impairment in heart failure results from reduced BAG3-mediated sarcomeric protein turnover. *Nat. Commun.* **12**, 2942 (2021).
7. Lange, S., Pinotsis, N., Agarkova, I. & Ehler, E. The M-band: the underestimated part of the sarcomere. *Biochim. Biophys. Acta Mol. Cell Res.* **1867**, 118440 (2020).
8. Lange, S. et al. The kinase domain of titin controls muscle gene expression and protein turnover. *Science* **308**, 1599–1603 (2005).
9. Solaro, R. J. Multiplex kinase signaling modifies cardiac function at the level of sarcomeric proteins. *J. Biol. Chem.* **283**, 26829–26833 (2008).
10. Hu, L.-Y. R., Ackermann, M. A. & Kontrogianni-Konstantopoulos, A. The sarcomeric M-region: a molecular command center for diverse cellular processes. *Biomed. Res. Int.* **2015**, 714197 (2015).
11. Wallimann, T., Doetschman, T. C. & Eppenberger, H. M. Novel staining pattern of skeletal muscle M-lines upon incubation with antibodies against MM-creatine kinase. *J. Cell Biol.* **96**, 1772–1779 (1983).
12. Lange, S. et al. Subcellular targeting of metabolic enzymes to titin in heart muscle may be mediated by DRAL/FHL-2. *J. Cell Sci.* **115**, 4925–4936 (2002).
13. Almomani, R. et al. Biallelic truncating mutations in ALPK3 cause severe pediatric cardiomyopathy. *J. Am. Coll. Cardiol.* **67**, 515–525 (2016).
14. Aung, N. et al. Genome-wide analysis of left ventricular image-derived phenotypes identifies fourteen loci associated with cardiac morphogenesis and heart failure development. *Circulation* **140**, 1318–1330 (2019).
15. Herkert, J. C. et al. Expanding the clinical and genetic spectrum of ALPK3 variants: phenotypes identified in pediatric cardiomyopathy patients and adults with heterozygous variants. *Am. Heart J.* **225**, 108–119 (2020).
16. Lopes, L. R. et al. Alpha-protein kinase 3 (ALPK3) truncating variants are a cause of autosomal dominant hypertrophic cardiomyopathy. *Eur. Heart J.* **42**, 3063–3073 (2021).
17. Phelan, D. G. et al. ALPK3-deficient cardiomyocytes generated from patient-derived induced pluripotent stem cells and mutant human embryonic stem cells display abnormal calcium handling and establish that ALPK3 deficiency underlies familial cardiomyopathy. *Eur. Heart J.* **37**, 2586–2590 (2016).
18. Van Sligtenhorst, I. et al. Cardiomyopathy in α -kinase 3 (ALPK3)-deficient mice. *Vet. Pathol.* **49**, 131–141 (2012).
19. Middelbeek, J., Clark, K., Venselaar, H., Huynen, M. A. & van Leeuwen, F. N. The alpha-kinase family: an exceptional branch on the protein kinase tree. *Cell. Mol. Life Sci.* **67**, 875–890 (2010).
20. Hosoda, T. et al. A novel myocyte-specific gene Midori promotes the differentiation of P19CL6 cells into cardiomyocytes. *J. Biol. Chem.* **276**, 35978–35989 (2001).
21. Agarwal, R. et al. Pathogenesis of cardiomyopathy caused by variants in ALPK3, an essential pseudokinase in the cardiomyocyte nucleus and sarcomere. *Circulation* **146**, 1674–1693 (2022).
22. Kuczumski, E. R. & Spudich, J. A. Regulation of myosin self-assembly: phosphorylation of *Dictyostelium* heavy chain inhibits formation of thick filaments. *Proc. Natl Acad. Sci. USA* **77**, 7292–7296 (1980).
23. Liu, W. J. et al. p62 links the autophagy pathway and the ubiquitin-proteasome system upon ubiquitinated protein degradation. *Cell. Mol. Biol. Lett.* **21**, 29 (2016).
24. Pankiv, S. et al. p62/SQSTM1 binds directly to Atg8/LC3 to facilitate degradation of ubiquitinated protein aggregates by autophagy. *J. Biol. Chem.* **282**, 24131–24145 (2007).
25. Sim, C. B. et al. Sex-specific control of human heart maturation by the progesterone receptor. *Circulation* **143**, 1614–1628 (2021).
26. McKellar, D. W. et al. Large-scale integration of single-cell transcriptomic data captures transitional progenitor states in mouse skeletal muscle regeneration. *Commun. Biol.* **4**, 1280 (2021).
27. Hofsteen, P. et al. ALPK2 promotes cardiogenesis in zebrafish and human pluripotent stem cells. *iScience* **2**, 88–100 (2018).
28. Mills, R. J. et al. Functional screening in human cardiac organoids reveals a metabolic mechanism for cardiomyocyte cell cycle arrest. *Proc. Natl Acad. Sci. USA* **114**, E8372–E8381 (2017).
29. Musa, H. et al. Targeted homozygous deletion of M-band titin in cardiomyocytes prevents sarcomere formation. *J. Cell Sci.* **119**, 4322–4331 (2006).
30. Hornemann, T. et al. Muscle-type creatine kinase interacts with central domains of the M-band proteins myomesin and M-protein. *J. Mol. Biol.* **332**, 877–887 (2003).
31. Singh, S. R. et al. Activation of autophagy ameliorates cardiomyopathy in *Mybpc3*-targeted knockin mice. *Circ. Heart Fail.* **10**, e004140 (2017).
32. Hoffman, N. J. et al. Global phosphoproteomic analysis of human skeletal muscle reveals a network of exercise-regulated kinases and AMPK substrates. *Cell Metab.* **22**, 922–935 (2015).
33. Knight, J. D. et al. A novel whole-cell lysate kinase assay identifies substrates of the p38 MAPK in differentiating myoblasts. *Skelet. Muscle* **2**, 5 (2012).
34. Wu, G. et al. Truncating variants in *OBSCN* gene associated with disease-onset and outcomes of hypertrophic cardiomyopathy. *Circ. Genom. Precis. Med.* **14**, e003401 (2021).
35. Blondelle, J. et al. Murine obscurin and Obsl1 have functionally redundant roles in sarcolemmal integrity, sarcoplasmic reticulum organization, and muscle metabolism. *Commun. Biol.* **2**, 178 (2019).
36. Bucelli, R. C. et al. *SQSTM1* splice site mutation in distal myopathy with rimmed vacuoles. *Neurology* **85**, 665–674 (2015).
37. Dadson, K. et al. The E3 ligase Mule protects the heart against oxidative stress and mitochondrial dysfunction through Myc-dependent inactivation of Pgc-1 α and Pink1. *Sci. Rep.* **7**, 41490 (2017).
38. Lyon, R. C., Zanella, F., Omens, J. H. & Sheikh, F. Mechanotransduction in cardiac hypertrophy and failure. *Circ. Res.* **116**, 1462–1476 (2015).
39. Buyandelger, B. et al. MLP (muscle LIM protein) as a stress sensor in the heart. *Pflugers Arch.* **462**, 135–142 (2011).
40. Knöll, R. et al. The cardiac mechanical stretch sensor machinery involves a Z disc complex that is defective in a subset of human dilated cardiomyopathy. *Cell* **111**, 943–955 (2002).
41. Purcell, N. H. et al. Extracellular signal-regulated kinase 2 interacts with and is negatively regulated by the LIM-only protein FHL2 in cardiomyocytes. *Mol. Cell. Biol.* **24**, 1081–1095 (2004).
42. Miller, G., Musa, H., Gautel, M. & Peckham, M. A targeted deletion of the C-terminal end of titin, including the titin kinase domain, impairs myofibrillogenesis. *J. Cell Sci.* **116**, 4811–4819 (2003).
43. Perera, S., Holt, M. R., Mankoo, B. S. & Gautel, M. Developmental regulation of MURF ubiquitin ligases and autophagy proteins nbr1, p62/SQSTM1 and LC3 during cardiac myofibril assembly and turnover. *Dev. Biol.* **351**, 46–61 (2011).
44. Willis, M. S. & Patterson, C. Proteotoxicity and cardiac dysfunction—Alzheimer’s disease of the heart? *N. Engl. J. Med.* **368**, 455–464 (2013).
45. Henning, R. H. & Brundel, B. J. J. M. Proteostasis in cardiac health and disease. *Nat. Rev. Cardiol.* **14**, 637–653 (2017).
46. Dorsch, L. M. et al. Protein quality control activation and microtubule remodeling in hypertrophic cardiomyopathy. *Cells* **8**, 741 (2019).
47. Gilda, J. E. & Gomes, A. V. Proteasome dysfunction in cardiomyopathies. *J. Physiol.* **595**, 4051–4071 (2017).

48. Mehdiabadi, N. R. et al. Defining the fetal gene program at single-cell resolution in pediatric dilated cardiomyopathy. *Circulation* **146**, 1105–1108 (2022).
49. McGinnis, C. S., Murrow, L. M. & Gartner, Z. J. DoubletFinder: doublet detection in single-cell RNA sequencing data using artificial nearest neighbors. *Cell Syst.* **8**, 329–337 (2019).
50. Stuart, T. et al. Comprehensive integration of single-cell data. *Cell* **177**, 1888–1902 (2019).
51. Butler, A., Hoffman, P., Smibert, P., Papalexi, E. & Satija, R. Integrating single-cell transcriptomic data across different conditions, technologies, and species. *Nat. Biotechnol.* **36**, 411–420 (2018).
52. Stuart, T. & Satija, R. Integrative single-cell analysis. *Nat. Rev. Genet.* **20**, 257–272 (2019).
53. Richards, M., Fong, C.-Y., Chan, W.-K., Wong, P.-C. & Bongso, A. Human feeders support prolonged undifferentiated growth of human inner cell masses and embryonic stem cells. *Biotechnol.* **20**, 933–936 (2002).
54. Elliott, D. A. et al. NKX2-5^{eGFP/w} hESCs for isolation of human cardiac progenitors and cardiomyocytes. *Nat. Methods* **8**, 1037–1040 (2011).
55. Humphrey, S. J., Karayel, O., James, D. E. & Mann, M. High-throughput and high-sensitivity phosphoproteomics with the EasyPhos platform. *Nat. Protoc.* **13**, 1897–1916 (2018).
56. Bruderer, R. et al. Extending the limits of quantitative proteome profiling with data-independent acquisition and application to acetaminophen-treated three-dimensional liver microtissues. *Mol. Cell. Proteomics* **14**, 1400–1410 (2015).
57. Tyanova, S. et al. The Perseus computational platform for comprehensive analysis of (prote)omics data. *Nat. Methods* **13**, 731–740 (2016).
58. Jiang, H., Lei, R., Ding, S.-W. & Zhu, S. Skewer: a fast and accurate adapter trimmer for next-generation sequencing paired-end reads. *BMC Bioinformatics* **15**, 182 (2014).
59. Dobin, A. et al. STAR: ultrafast universal RNA-seq aligner. *Bioinformatics* **29**, 15–21 (2013).
60. Liao, Y., Smyth, G. K. & Shi, W. featureCounts: an efficient general purpose program for assigning sequence reads to genomic features. *Bioinformatics* **30**, 923–930 (2014).
61. Robinson, M. D. & Oshlack, A. A scaling normalization method for differential expression analysis of RNA-seq data. *Genome Biol.* **11**, R25 (2010).
62. Benjamini, Y. & Hochberg, Y. Controlling the false discovery rate: a practical and powerful approach to multiple testing. *J. R. Stat. Soc. B Methodol.* **57**, 289–300 (1995).
63. Mills, R. J. et al. Drug screening in human PSC-cardiac organoids identifies pro-proliferative compounds acting via the mevalonate pathway. *Cell Stem Cell* **24**, 895–907 (2019).

Acknowledgements

We thank the National Health and Medical Research Council of Australia (E.R.P., D.A.E., B.L.P.; grant nos. GNT2008376, 1160256 and 1160257), the Australian Research Council (E.R.P.; grant no. DP190101972), the Heart Foundation of Australia (E.R.P., D.A.E.; grant nos. 104997 and 105146), the Medical Research Future Fund (E.R.P., D.A.E.; grant nos. MRF2007316 and MRF2007471), the Stafford Fox Medical Research Foundation (E.R.P.), the Australian Genomics Health Alliance (J.W.M., E.R.P., D.A.E.), the Royal Children's Hospital Foundation (E.R.P.) and the Murdoch Children's Research Institute (MCRI) Early Career Researcher Award (J.W.M.) for grant and fellowship support. The MCRI is supported by the Victorian Government's Operational Infrastructure Support Program. E.R.P. and D.A.E. are principal investigators of the Novo Nordisk Foundation Center for Stem Cell Medicine, which is supported by Novo Nordisk Foundation grant no. NNF21CC0073729. L.R.L. is supported by a UK

Research and Innovation Medical Research Council clinical academic research partnership award (no. MR/T005181/1). The generation of the *Alpk3*^{W1538X} mice used in this study was supported by Phenomics Australia and the Australian Government through the National Collaborative Research Infrastructure Strategy program. The funders had no role in study design, data collection and analysis, decision to publish or preparation of the manuscript.

Author contributions

J.W.M., E.R.P. and D.A.E. conceived the project. J.W.M., F.B., A.T.L.Z., K.K., H.L.P. and K.I.W. contributed to cell line generation and validation, cardiac differentiation, confocal microscopy, generation of RNA and protein samples and western blotting. J.W.M., B.L.P. and J.M. generated and analyzed the proteomics and phosphoproteomics data. H.K.V., R.J.M. and J.E.H. collected and analyzed the hCO data. N.R.M., N.C. and M.R. analyzed the RNA-seq dataset. J.W.M. and F.A. collected and analyzed all mouse echocardiography data. J.D.C. and G.S.L. generated data using iPSC-derived skeletal muscle cells. P.S., L.R.L. and P.M.E. provided key reagents and identified the patient-specific variants used. S.L. provided key reagents. J.W.M. compiled the final figures with contributions from the other authors. J.W.M., E.R.P. and D.A.E. wrote the manuscript. All authors approved the final version of the manuscript.

Competing interests

R.J.M., J.E.H. and E.R.P. are cofounders, scientific advisors and hold equity in Dynamics, a biotechnology company focused on the development of heart failure therapeutics. The other authors declare no competing interests.

Additional information

Extended data is available for this paper at <https://doi.org/10.1038/s44161-023-00219-9>.

Supplementary information The online version contains supplementary material available at <https://doi.org/10.1038/s44161-023-00219-9>.

Correspondence and requests for materials should be addressed to Enzo R. Porrello or David A. Elliott.

Peer review information *Nature Cardiovascular Research* thanks Mark Mercola and the other, anonymous, reviewer(s) for their contribution to the peer review of this work.

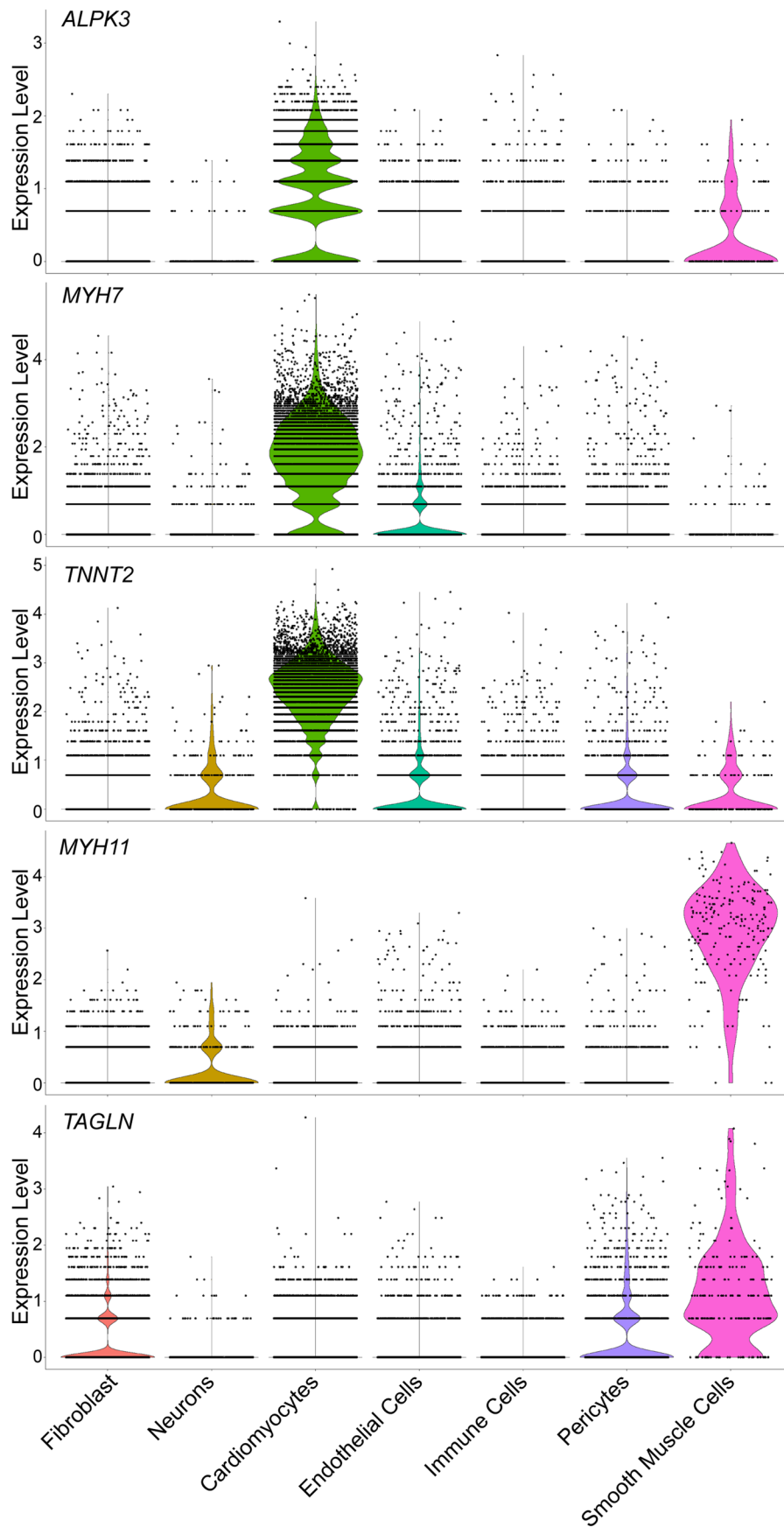
Reprints and permissions information is available at www.nature.com/reprints.

Publisher's note Springer Nature remains neutral with regard to jurisdictional claims in published maps and institutional affiliations.

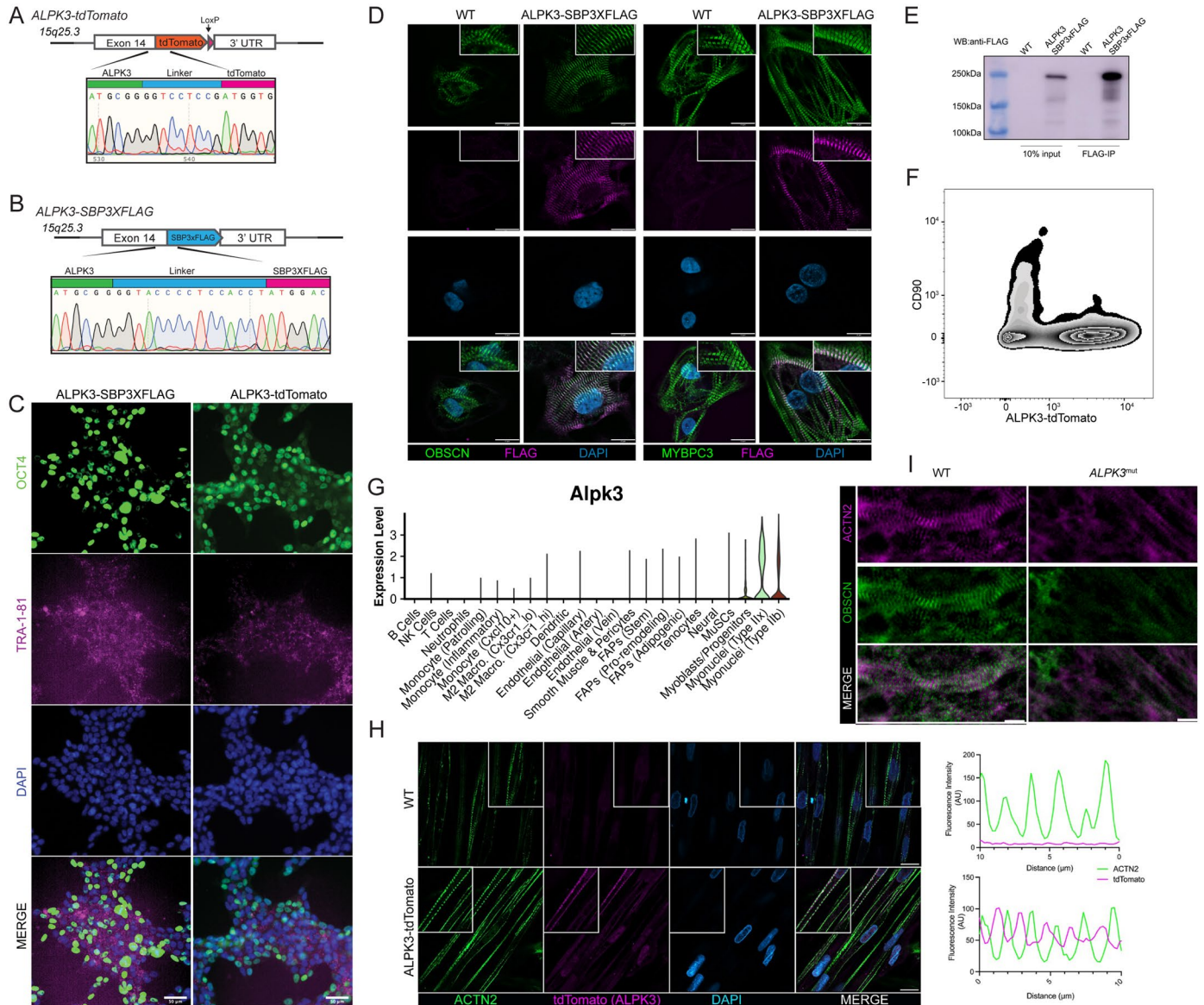
Open Access This article is licensed under a Creative Commons Attribution 4.0 International License, which permits use, sharing, adaptation, distribution and reproduction in any medium or format, as long as you give appropriate credit to the original author(s) and the source, provide a link to the Creative Commons license, and indicate if changes were made. The images or other third party material in this article are included in the article's Creative Commons license, unless indicated otherwise in a credit line to the material. If material is not included in the article's Creative Commons license and your intended use is not permitted by statutory regulation or exceeds the permitted use, you will need to obtain permission directly from the copyright holder. To view a copy of this license, visit <http://creativecommons.org/licenses/by/4.0/>.

© The Author(s) 2023

¹Murdoch Children's Research Institute, Royal Children's Hospital, Melbourne, Victoria, Australia. ²Melbourne Centre for Cardiovascular Genomics and Regenerative Medicine, Royal Children's Hospital, Melbourne, Victoria, Australia. ³Department of Anatomy and Physiology, University of Melbourne, Melbourne, Victoria, Australia. ⁴Centre for Muscle Research, University of Melbourne, Melbourne, Victoria, Australia. ⁵Novo Nordisk Foundation Centre for Stem Cell Medicine (reNEW), Murdoch Children's Research Institute, Melbourne, Victoria, Australia. ⁶School of Biomedical Sciences and Department of Paediatrics, University of Melbourne, Melbourne, Victoria, Australia. ⁷Precision Cardiovascular Laboratory, The University of Sydney, Sydney, New South Wales, Australia. ⁸Australian Regenerative Medicine Institute, Monash University, Melbourne, Victoria, Australia. ⁹Centre for Heart Muscle Disease, Institute of Cardiovascular Science, University College London, London, UK. ¹⁰Barts Heart Centre, St. Bartholomew's Hospital, Barts Health NHS Trust, London, UK. ¹¹Queensland Institute of Medical Research Berghofer Medical Research Institute, Brisbane, Queensland, Australia. ¹²Present address: Australian Regenerative Medicine Institute, Monash University, Melbourne, Victoria, Australia. ¹³Present address: Novo Nordisk Foundation Centre for Stem Cell Medicine (reNEW), Murdoch Children's Research Institute, Melbourne, Victoria, Australia. ¹⁴These authors contributed equally: Enzo R. Porrello, David A. Elliott. ✉e-mail: enzo.porrello@mcri.edu.au; David.elliott@mcri.edu.au

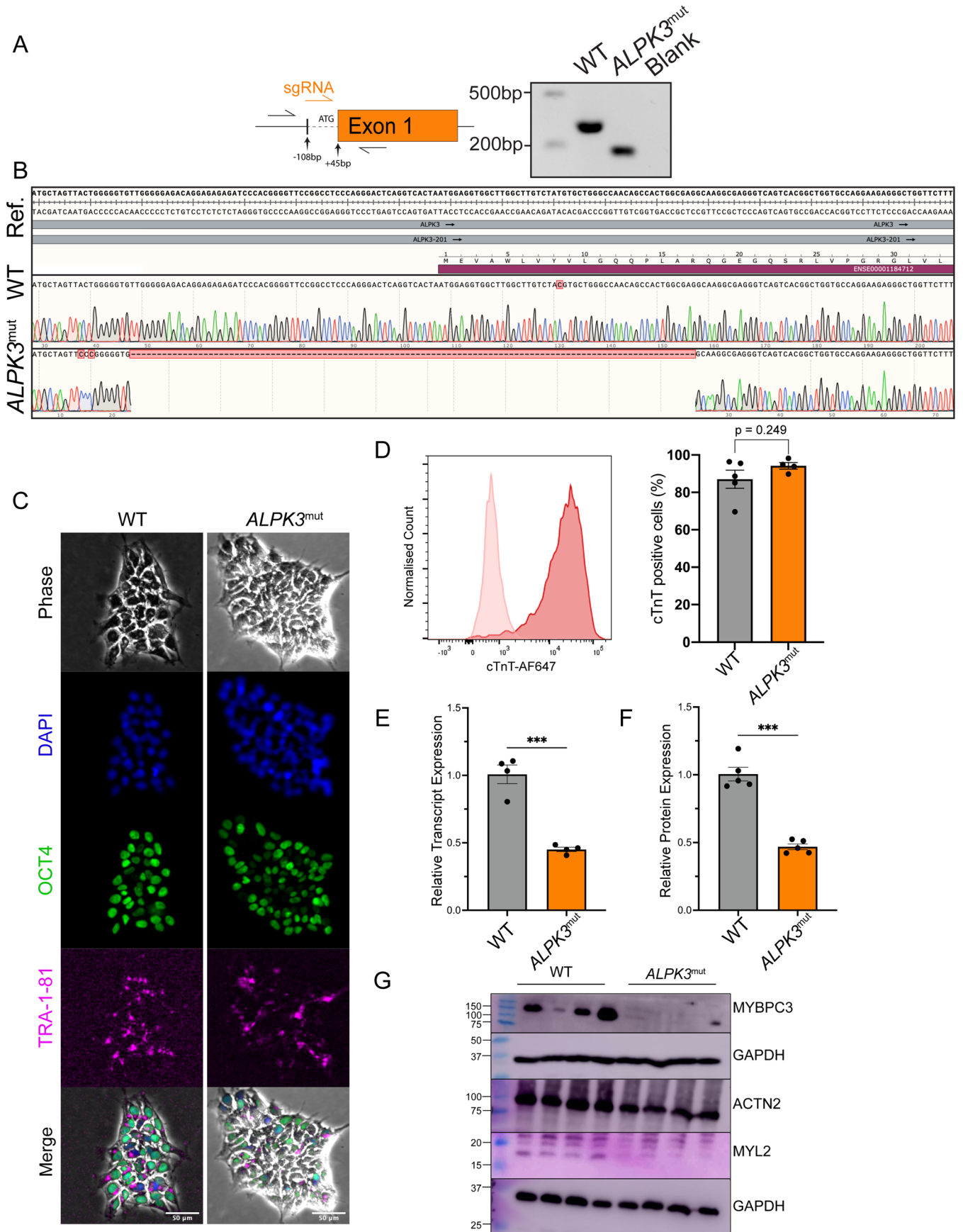


Extended Data Fig. 1 | Single nucleus RNA sequencing. Violin plot of *ALPK3*, cardiomyocyte markers *MYH7* and *TNNT2*, and smooth muscle cell markers *MYH11* and *TAGLN*. n = 3 adult hearts.



Extended Data Fig. 2 | Validation of C-terminal tagged *ALPK3* hPSC cell lines. **a.** Gene targeting outline of *ALPK3-tdTomato* hPSC cell line and Sanger sequencing confirmation of junction. **b.** Gene targeting outline of *ALPK3-SBP3xFLAG* hPSC cell line and Sanger sequencing confirmation of junction of gene fusion. **c.** Stem cell markers of *ALPK3-SBP3xFLAG* and *ALPK3-tdTomato* hPSC cell lines. Scale bar = 50 μ m. **d.** Representative immunofluorescent micrograph of *ALPK3-SBP3xFLAG* and WT hPSC-CM's stained for OBSCN (green), FLAG (magenta), and DAPI (blue) or MYBPC3 (green), FLAG (magenta), and DAPI (blue). Scale bar = 20 μ m. **e.** Western blot of WT and *ALPK3-SBP3xFLAG*

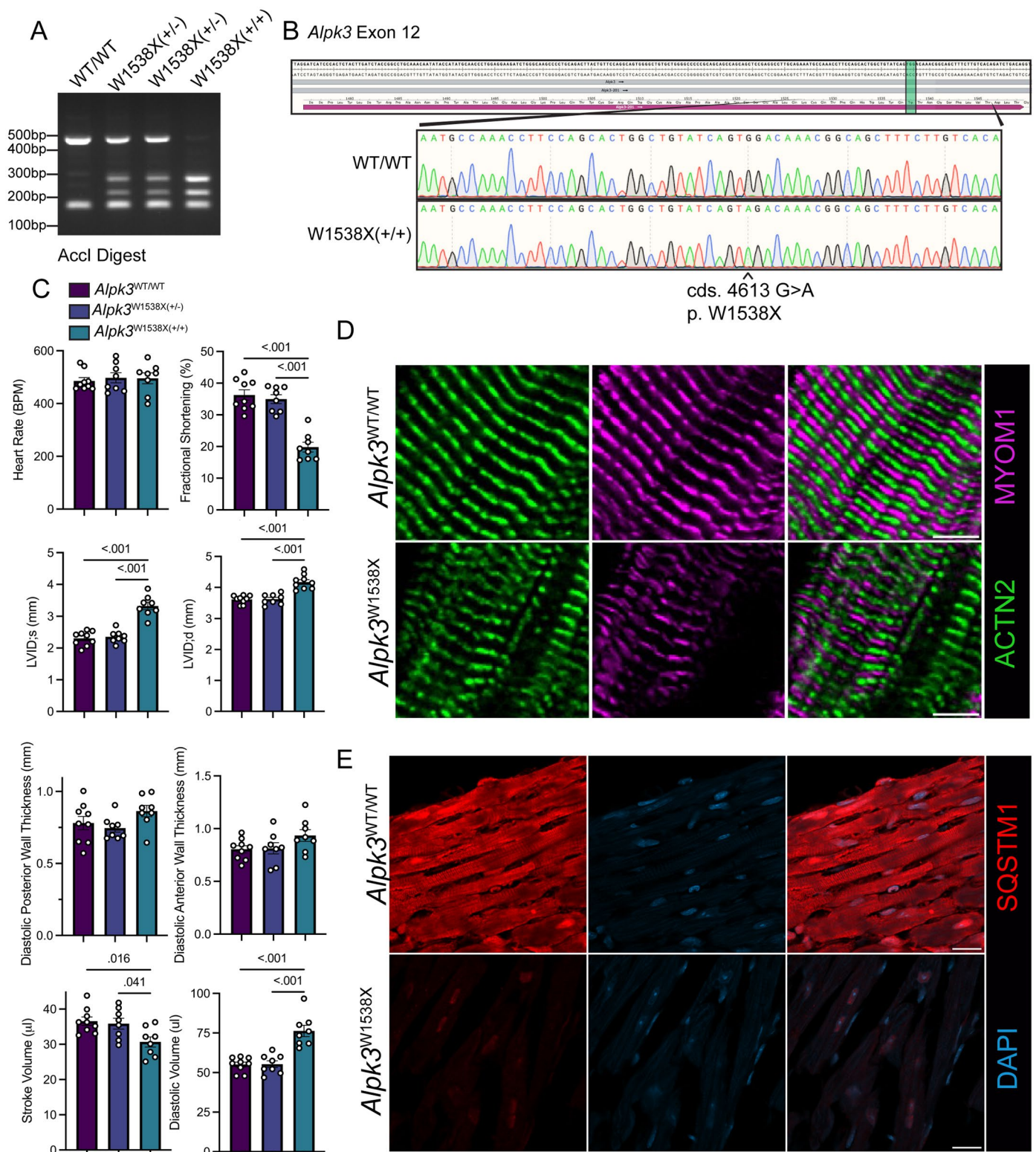
hPSC-CMs immunoprecipitated with anti-FLAG antibody. **f.** Flow cytometry of *ALPK3-tdTomato* stained for stromal cell marker CD90. **g.** Violin plot of *ALPK3* expression across 23 cell types identified in mouse skeletal muscle. **h.** Representative immunofluorescent micrograph of WT and *ALPK3-tdTomato* hPSC-skeletal muscle stained for alpha-actinin (green), tdTomato (magenta), and DAPI. Scale bar = 15 μ m. Line profile demonstrating alpha-actinin and *ALPK3*tdTomato organization. **i.** Immunofluorescence of WT and *ALPK3*mut hCOs staining alpha-actinin (magenta) and obscurin (green), scale bar = 10 μ m.



Extended Data Fig. 3 | See next page for caption.

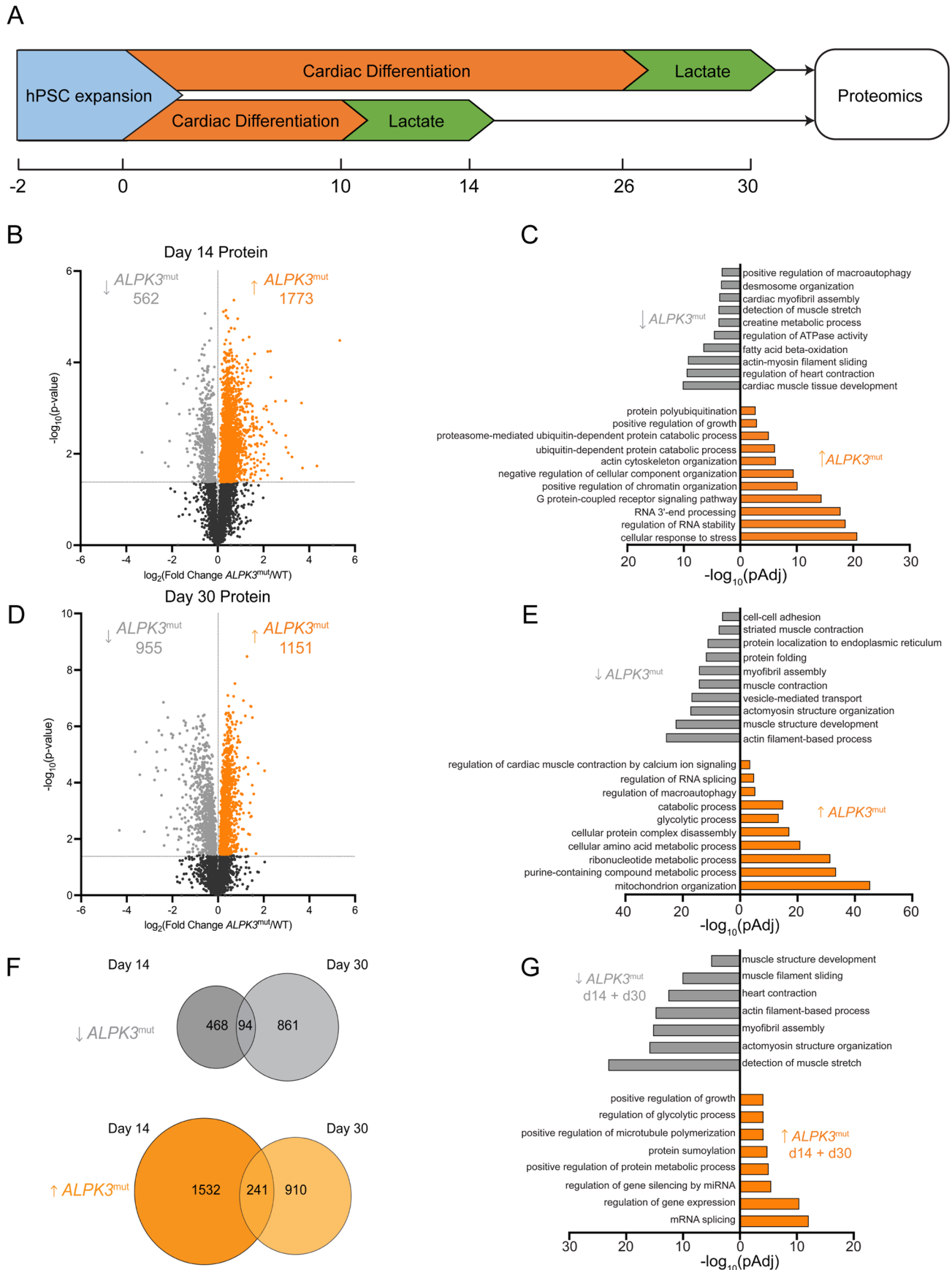
Extended Data Fig. 3 | Validation of *ALPK3*^{mut} hPSC cell line. **a** Gene targeting strategy with screening primers (black) and gRNA location (orange). PCR genotyping gel. **b** Sanger sequencing chromatograms of WT and *ALPK3*^{mut} amplicons against reference human genome. **c** Stem cell markers of WT and *ALPK3*^{mut} hPSC cell lines. Scale bar = 50 μ m. **d** Flow cytometry of WT and *ALPK3*^{mut} hPSC-CMs using cardiac troponin-T. n = 5 for WT and 4 for *ALPK3*^{mut}. Data is presented as mean \pm S.E.M. Two-sided t-test. **e** Relative *ALPK3* RNAseq transcript

levels by for day 30 purified WT and *ALPK3*^{mut} hPSC-CMs. n = 4 biological replicates. *** indicates $p < 0.001$ from two-sided t-test. Data is presented as mean \pm S.E.M. **f** Relative ALPK3 protein levels by mass spectrometry for day 30 purified WT and *ALPK3*^{mut} hPSC-CMs. n = 5 biological replicates. *** indicates $p < 0.001$ from two-sided t-test. Data is presented as mean \pm S.E.M. **g** Western blot of select sarcomeric proteins between day 30 purified WT and *ALPK3*^{mut} hPSC-CMs.



Extended Data Fig. 4 | Generation and characterization of $Alpk3^{W1538X}$ mouse model. **a** Representative AccI digest of genotyping PCR products from $Alpk3^{WT/WT}$, $Alpk3^{W1538X(+/-)}$, and $Alpk3^{W1538X(+/+)}$ mice. **b** Sanger sequencing chromatograms of WT and $Alpk3^{W1538X(+/-)}$ mice against reference c57/Bl6 mouse *Alpk3* gene. **c** Summary echocardiography data (continued from Fig. 3i) of 6-week-old mice showing heart rate, left ventricular diastolic and systolic internal diameter, fractional shortening, diastolic posterior and anterior wall thickness, stroke

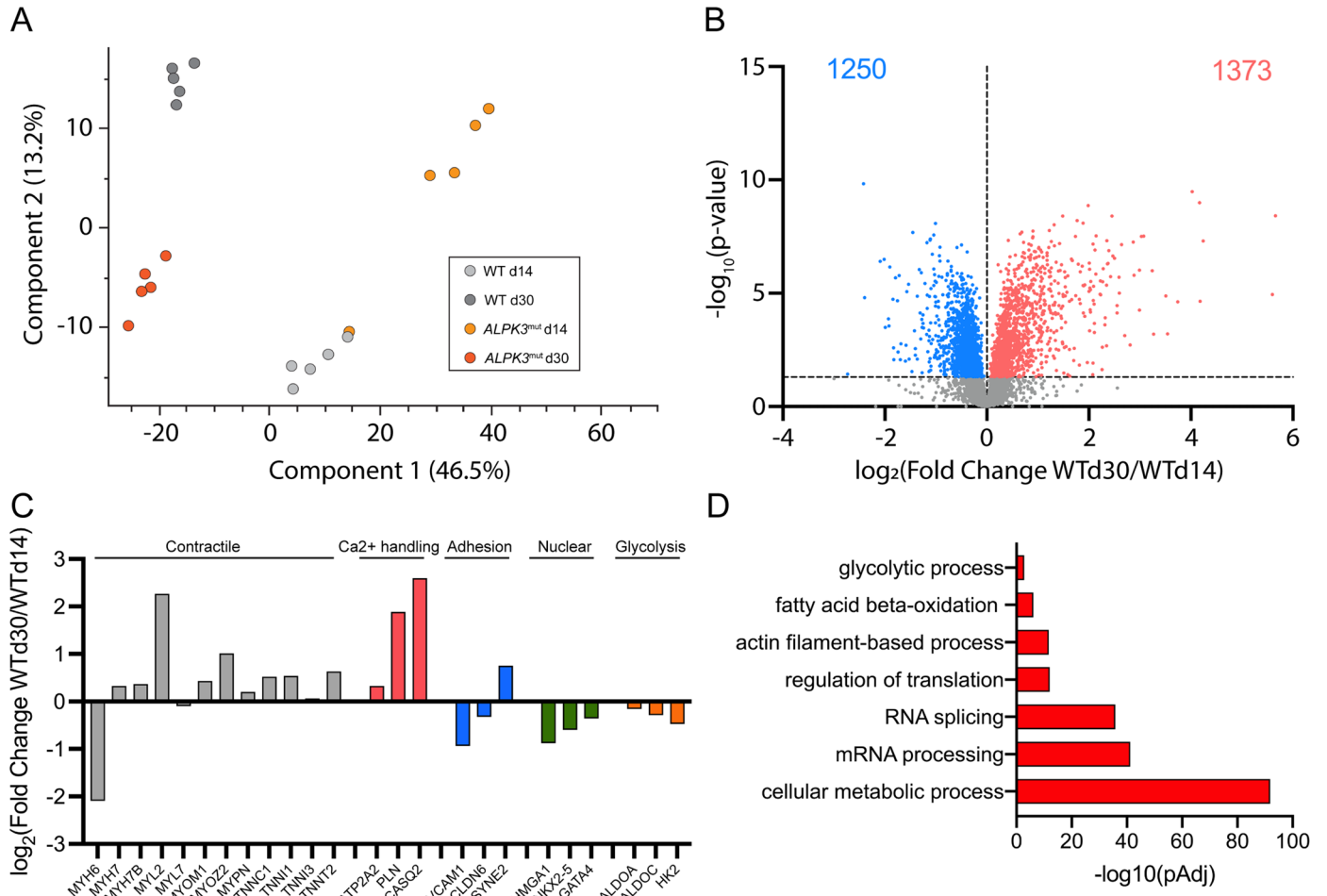
volume, and diastolic volume. Statistical significance established by ordinary one-way ANOVA with Tukey's multiple comparison test. Error bars represent S.E.M. **d** Immunofluorescent staining of ACTN2 (green) and MYOM1 (magenta) in 21-day-old $Alpk3^{WT/WT}$ and $Alpk3^{W1538X(+/-)}$ mouse hearts. Scale bar = 5 μ m. **e** Immunofluorescent staining of SQSTM1 (red) and DAPI (blue) in 21-day-old $Alpk3^{WT/WT}$ and $Alpk3^{W1538X(+/+)}$ mouse hearts. Scale bar = 15 μ m.



Extended Data Fig. 5 | See next page for caption.

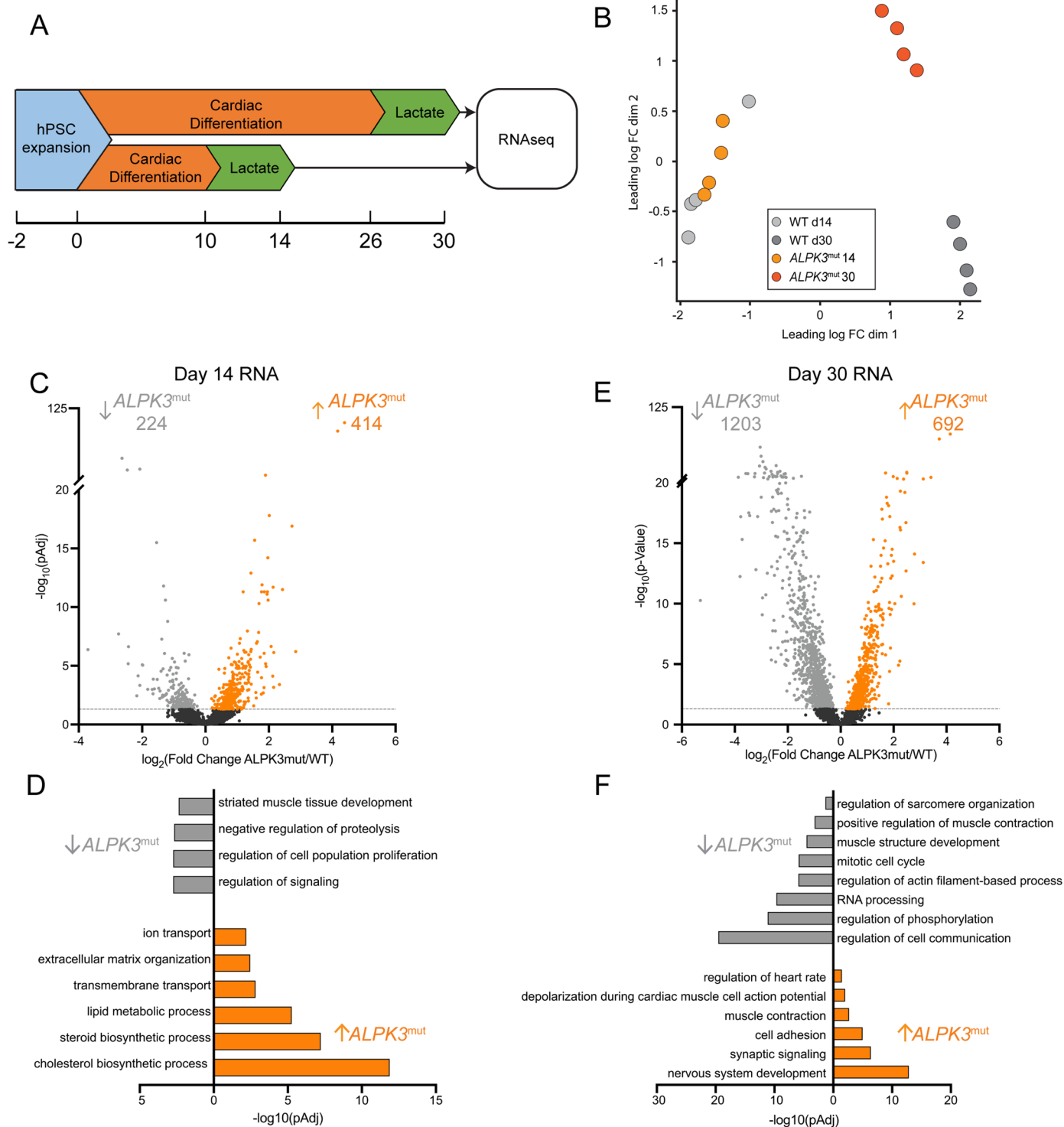
Extended Data Fig. 5 | ALPK3 deficient cardiomyocytes have compromised expression of key cardiac protein networks. **a** Experimental outline of proteomics experiment. n = 5 per group. **b** Volcano plot of day 14 WT and *ALPK3*^{mut} hPSC-CMs to show differential protein expression. **c** Gene ontology (GO) of biological processes enriched in differentially expressed proteins in day 14 WT and *ALPK3*^{mut} hPSC-CMs. **d** Volcano plot of day 30 WT and *ALPK3*^{mut}

hPSC-CMs to show differential protein expression. **e** GO of biological processes enriched in differentially expressed proteins in day 30 WT and *ALPK3*^{mut} hPSC-CMs. **f** Venn diagrams of protein expression up- or down-regulated proteins common for day 14 and day 30. **g** GO of biological processes of commonly up- or down-regulated proteins in *ALPK3*^{mut} hPSC-CMs.



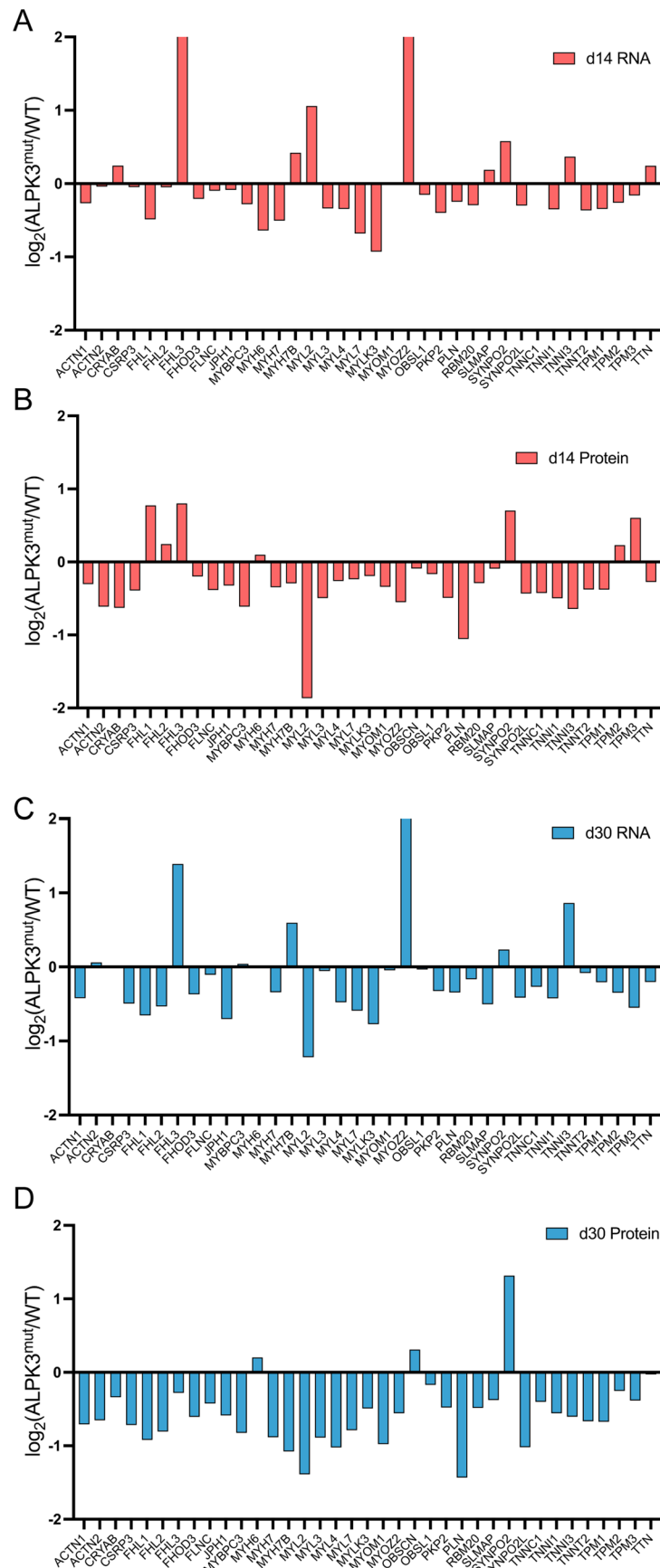
Extended Data Fig. 6 | Proteomic profile of day 14 vs. day 30 WT hPSC-CMs. **a** Principal component analysis plot of day 14 and day 30 purified WT and *ALPK3*^{mut} hPSC-CMs. **b** Volcano plot of proteins demonstrating log fold change of day 30 proteins vs. day 14 proteins in WT hPSC-CMs. **c** Protein expression profile of

select contractile, calcium handling, adhesion, nuclear, and glycolytic proteins at day 30 vs. day 14. **d** GO term biological processes associated with changes in protein between day 30 and day 14 WT hPSC-CMs.



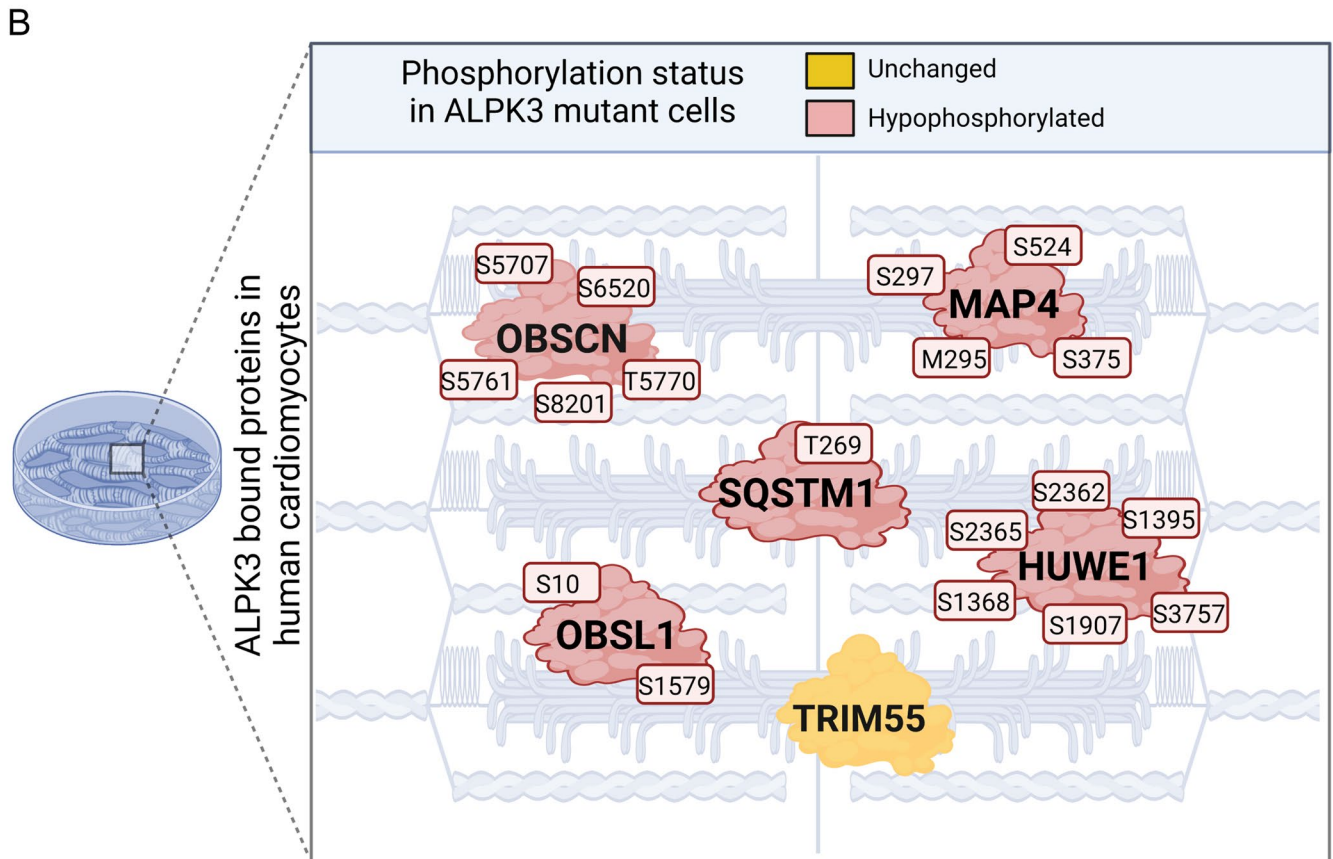
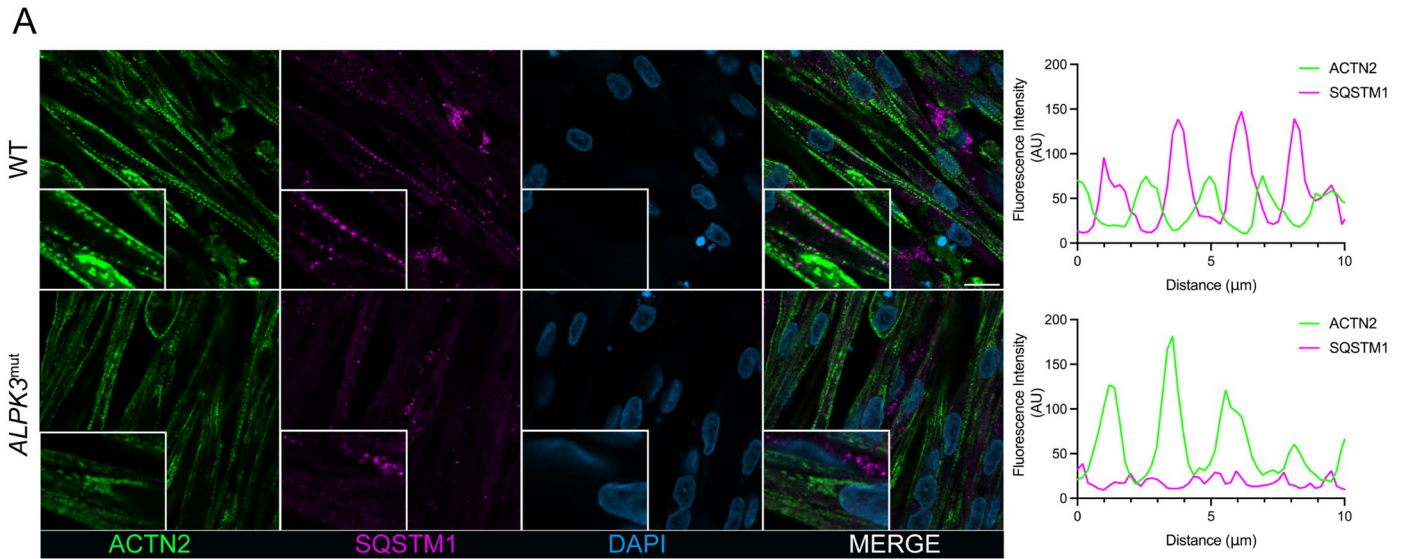
Extended Data Fig. 7 | RNA sequencing of purified WT and ALPK3^{mut} hPSC-CMs. a Experimental outline. n = 4 per group. **b** Principal component analysis of day 14 and 30 WT and ALPK3^{mut} hPSC-CMs. **c** Volcano plot of transcript levels between day 14 ALPK3^{mut} and WT hPSC-CMs. **d** GO term analysis of enriched biological processes of differentially expressed transcripts between day 14

ALPK3^{mut} and WT hPSC-CMs. **e** Volcano plot of transcript levels between day 30 ALPK3^{mut} and WT hPSC-CMs. **f** GO term analysis of enriched biological processes of differentially expressed transcripts between day 30 ALPK3^{mut} and WT hPSC-CMs.



Extended Data Fig. 8 | Comparison of RNA and protein expression of contractile proteins in WT and $\text{ALPK3}^{\text{mut}}$ purified hPSC-CMs at two timepoints. a. Logarithmic change of RNA transcript levels between day 14 WT and $\text{ALPK3}^{\text{mut}}$ hPSC-CMs. $n = 4$ per group. **b.** Logarithmic change of protein

levels between day 14 WT and $\text{ALPK3}^{\text{mut}}$ hPSC-CMs. $n = 5$ per group. **c.** Logarithmic change of RNA transcript levels between day 30 WT and $\text{ALPK3}^{\text{mut}}$ hPSC-CMs. $n = 4$ per group. **d.** Logarithmic change of protein levels between day 30 WT and $\text{ALPK3}^{\text{mut}}$ hPSC-CMs. $n = 5$ per group.



Extended Data Fig. 10 | SQSTM1 localization in WT and *ALPK3*^{mut} hPSC-derived skeletal muscle cells. **a.** Immunofluorescent micrograph of WT and *ALPK3*^{mut} hPSC-skeletal muscle stained for alpha actinin (green), SQSTM1 (magenta), and DAPI (blue). Scale bar = 15 μm. Line profile demonstrating alpha

actinin and SQSTM1 organization. **b.** Graphical representation of select proteins bound to ALPK3 which also showed reduced phosphopeptide abundance in *ALPK3*^{mut} hPSC-CMs. The affected phosphorylation sites are also highlighted. Created with BioRender.com.

Reporting Summary

Nature Portfolio wishes to improve the reproducibility of the work that we publish. This form provides structure for consistency and transparency in reporting. For further information on Nature Portfolio policies, see our [Editorial Policies](#) and the [Editorial Policy Checklist](#).

Statistics

For all statistical analyses, confirm that the following items are present in the figure legend, table legend, main text, or Methods section.

n/a Confirmed

- The exact sample size (n) for each experimental group/condition, given as a discrete number and unit of measurement
- A statement on whether measurements were taken from distinct samples or whether the same sample was measured repeatedly
- The statistical test(s) used AND whether they are one- or two-sided
Only common tests should be described solely by name; describe more complex techniques in the Methods section.
- A description of all covariates tested
- A description of any assumptions or corrections, such as tests of normality and adjustment for multiple comparisons
- A full description of the statistical parameters including central tendency (e.g. means) or other basic estimates (e.g. regression coefficient) AND variation (e.g. standard deviation) or associated estimates of uncertainty (e.g. confidence intervals)
- For null hypothesis testing, the test statistic (e.g. F , t , r) with confidence intervals, effect sizes, degrees of freedom and P value noted
Give P values as exact values whenever suitable.
- For Bayesian analysis, information on the choice of priors and Markov chain Monte Carlo settings
- For hierarchical and complex designs, identification of the appropriate level for tests and full reporting of outcomes
- Estimates of effect sizes (e.g. Cohen's d , Pearson's r), indicating how they were calculated

Our web collection on [statistics for biologists](#) contains articles on many of the points above.

Software and code

Policy information about [availability of computer code](#)

Data collection

Imaging data were collected using ZEISS ZEN 2012 (blue edition) or ZEISS ZEN Black software (version 2.3 SPI) (Zeiss Microscopy, Thornwood, NY) software installed on a ZEISS LSM 780 confocal microscope. RNA sequencing data were collected with NovaSeq Control Software for the Illumina NovaSeq 6000 sequencing system. Flow cytometry data were collected using the BD LSR Fortessa X-20 Cell Analyser (BD Biosciences) and BD FACSDiva (v9.0.1). Proteomics samples were analysed on a Dionex 3500 nanoHPLC coupled to an Orbitrap Eclipse mass spectrometer (ThermoFischer Scientific).

Data analysis

Immunofluorescent and calcium images were processed ZEISS ZEN Black software (version 2.3 SPI) (Zeiss Microscopy, Thornwood, NY) and Fiji ImageJ (version: 2.3.0/1.53q). Flow cytometry was analyzed using BD FlowJo (v10.8.1). Human cardiac organoid force analysis was performed using a previously published MATLAB script (Mills, 2017). Proteomics data were analysed using Spectronaut (15.1.210713.50606) and Perseus (Tyanova, S. Nat. Methods 2016). Bulk RNA sequencing analysis was performed using Skewer (v0.2.2) for trimming, aligned with STAR aligner (v2.5.3a). Reads were analysed with featureCounts (subread 2.0.0). Differential gene expression analysis was performed in the R statistical programming language (v3.6.0) with the Bioconductor packages edgeR (v3.36.0).

For manuscripts utilizing custom algorithms or software that are central to the research but not yet described in published literature, software must be made available to editors and reviewers. We strongly encourage code deposition in a community repository (e.g. GitHub). See the Nature Portfolio [guidelines for submitting code & software](#) for further information.

Data

Policy information about [availability of data](#)

All manuscripts must include a [data availability statement](#). This statement should provide the following information, where applicable:

- Accession codes, unique identifiers, or web links for publicly available datasets
- A description of any restrictions on data availability
- For clinical datasets or third party data, please ensure that the statement adheres to our [policy](#)

All proteomics raw data have been deposited in PRIDE: PXD035535 (total and phosphoproteomics data of WT vs. ALPK3mut), or PXD035734 (ALPK3-SBP3XFLAG affinity purification), or PXD038544 (Global kinase assay) and will be made public following acceptance of the manuscript. RNA sequencing has been deposited to the Gene Expression Omnibus: GSE215304 and will be made public following acceptance of the manuscript. Source data are provided with this paper. Other data is available upon reasonable request.

Human research participants

Policy information about [studies involving human research participants and Sex and Gender in Research](#).

Reporting on sex and gender	<input type="text" value="N/A"/>
Population characteristics	<input type="text" value="N/A"/>
Recruitment	<input type="text" value="N/A"/>
Ethics oversight	<input type="text" value="N/A"/>

Note that full information on the approval of the study protocol must also be provided in the manuscript.

Field-specific reporting

Please select the one below that is the best fit for your research. If you are not sure, read the appropriate sections before making your selection.

Life sciences Behavioural & social sciences Ecological, evolutionary & environmental sciences

For a reference copy of the document with all sections, see nature.com/documents/nr-reporting-summary-flat.pdf

Life sciences study design

All studies must disclose on these points even when the disclosure is negative.

Sample size	Sample sizes were based on even group distribution and no statistical method was used to predetermine sample size owing to the exploratory nature of the study. Experiments included a minimum of 3 biological replicates per condition across multiple experiments. Biological replicates were classed as monolayer differentiations. Sample sizes are consistent with best practices in the field.
Data exclusions	Minimal data were excluded from the study. Individual human cardiac organoids were excluded from analyses if they met outlier criteria using Prism (Version 9.3.1) ROUT, Q=1%.
Replication	The results depicted in this manuscript are representative of observations and analyses made across multiple experiments, biological replicates, and technical replicates. Each experiment included a minimum of 3 biological replicates per condition. All replication attempts were successful.
Randomization	No randomization past blinding of experiments was performed in this study. Additional controlling of covariates were not relevant to this study.
Blinding	Proteomics and RNAseq experiments were performed with experimenters blinded to genotype. All mass spectrometry was analyzed blinded to condition. Human cardiac organoid experiments were not blinded due to the automated processes used to collect and analyze results. Where relevant, immunofluorescent images were scored by observers blinded to genotype. All animal studies were performed and analyzed blinded.

Reporting for specific materials, systems and methods

We require information from authors about some types of materials, experimental systems and methods used in many studies. Here, indicate whether each material, system or method listed is relevant to your study. If you are not sure if a list item applies to your research, read the appropriate section before selecting a response.

Materials & experimental systems

Methods

n/a	Involved in the study
<input type="checkbox"/>	<input checked="" type="checkbox"/> Antibodies
<input type="checkbox"/>	<input checked="" type="checkbox"/> Eukaryotic cell lines
<input checked="" type="checkbox"/>	<input type="checkbox"/> Palaeontology and archaeology
<input type="checkbox"/>	<input checked="" type="checkbox"/> Animals and other organisms
<input checked="" type="checkbox"/>	<input type="checkbox"/> Clinical data
<input checked="" type="checkbox"/>	<input type="checkbox"/> Dual use research of concern

n/a	Involved in the study
<input checked="" type="checkbox"/>	<input type="checkbox"/> ChIP-seq
<input type="checkbox"/>	<input checked="" type="checkbox"/> Flow cytometry
<input checked="" type="checkbox"/>	<input type="checkbox"/> MRI-based neuroimaging

Antibodies

Antibodies used

Anti-Sarcomeric Alpha Actinin antibody Abcam (ab68167) 1 in 100 flow cytometry; 1:1000 immunofluorescence; 1:5000 Western Blot
 Anti-Sarcomeric Alpha Actinin antibody Sigma-Aldrich (A7811) 1 in 100 flow cytometry; 1:1000 immunofluorescence; 1:5000 Western Blot
 Anti-MYOMI antibody Abeam (ab205618) 1 in 200 immunofluorescence
 Anti-OBSCN antibody Abeam (ab121652) 1 in 500 immunofluorescence
 Anti-SQSTM1 / p62 antibody Abeam (ab56416) 1 in 100 immunofluorescence ; 1 in 2,000 Western Blotting
 Anti-FLAG antibody Sigma-Aldrich (F1804) 1 in 300 immunofluorescence; 1 in 1,000 Western Blotting
 Anti-FLAG antibody Cell Signalling Technologies (14793) 1 in 500 immunofluorescence
 PE/Cy7 anti-human CD90 antibody Biolegend (328124) 1 in 100 flow cytometry
 Anti-Cardiac Troponin T antibody Abeam (ab8295) 1 in 100 flow cytometry
 Anti-MYBPC3 (E7) antibody Santa Cruz Biotechnologies (sc-137180) 1 in 300 immunofluorescence; 1 in 5,000 Western Blotting
 Anti-phosphoSQSTM1/p62 (Thr269/272) antibody Cell Signalling Technologies (13121) 1 in 1,000 Western Blotting
 Anti-SQSTM1/p62 antibody Sigma-Aldrich (P0067) 1 in 500 immunofluorescence

Validation

Antibodies were previously validated for immunofluorescence of human or mouse tissue either in the laboratories of ourselves or commercial suppliers.

Eukaryotic cell lines

Policy information about [cell lines and Sex and Gender in Research](#)

Cell line source(s)

All hPSC cell lines were derivatives of the female HES3 NKX-GFP reporter cell line (Elliott et al. Nature Methods 2011 Oct 23;8(12)). The HES3 cell line is available from WiCell (ES03), and was originally reported in Richards et al. Nature Biotechnology 2002 Sep;20(9):933-6.

HEK293FT were sourced from Invitrogen (Cat# R70007)

Authentication

hPSC lines are checked for pluripotency and genomic integrity by immunofluorescence of pluripotency markers and molecular karyotyping. HEK293FT were not authenticated.

Mycoplasma contamination

All cell lines confirmed negative for mycoplasma.

Commonly misidentified lines
(See [ICLAC](#) register)

No commonly misidentified cell lines were used.

Animals and other research organisms

Policy information about [studies involving animals; ARRIVE guidelines](#) recommended for reporting animal research, and [Sex and Gender in Research](#)

Laboratory animals

3-8 week-old C57BL/6J Mice edited to contain a variant (W1538X) in the ALPK3 gene, were used in this study. Mice were fed standard chow and water ad libitum, and maintained in a 12-hour light/12-hour dark cycle at ambient room temperature.

Wild animals

No wild animals were used in this study

Reporting on sex

Echocardiography experiments contained a mixed gender.
 WT: n=9 (3M, 6F)
 Het: n=8 (4M,4F)
 Hom: n=9 (5M, 4F)

Field-collected samples

No field collected samples were used in this study.

Ethics oversight

All experiments were approved by the Animal Ethics Committee of the Murdoch Children's Research Institute, Parkville, Australia

Note that full information on the approval of the study protocol must also be provided in the manuscript.

Plots

Confirm that:

- The axis labels state the marker and fluorochrome used (e.g. CD4-FITC).
- The axis scales are clearly visible. Include numbers along axes only for bottom left plot of group (a 'group' is an analysis of identical markers).
- All plots are contour plots with outliers or pseudocolor plots.
- A numerical value for number of cells or percentage (with statistics) is provided.

Methodology

Sample preparation

Flow cytometry of reporter line-derived hPSC-cardiomyocytes using endogenous fluorescence was performed following Trypsin-EDTA (0.25%), phenol red (ThermoFisher Scientific) for 5 minutes followed by inactivation with aMEM +10% FBS. Cell suspensions were filtered with 100um strainer to produce a single cell suspension and resuspended in PBS/2% FBS. For intracellular flow, cells were fixed in 2% paraformaldehyde (PFA) for 536 10 minutes prior to permeabilization with 0.25% triton X-100. Primary antibody staining used alpha-actinin (Sigma-Aldrich A7811 (Abcam ab11370) or cardiac troponin-T (ab8295). For surface staining of stromal cell populations, a PE-Cy7 conjugated anti-CD90 antibody was stained in PBS/2% FBS for 30 minutes in the dark at room temperature. Following staining, cells were washed 3 times with PBS/2% FBS and resuspended in PBS/2% FBS containing either DAPI or propidium iodide.

Instrument

Flow cytometry was performed using the BD LSR Fortessa X-20 Cell Analyzer (BD Biosciences, California, U.S.A.).

Software

Data acquisition and analysis was performed using FACSDiva versions 8.0.1 and 9.0.1 (BD Biosciences) and FlowJo Software.

Cell population abundance

Cardiac myocyte abundance was assessed using alpha-actinin (Sigma-Aldrich A7811 (Abcam ab11370) or cardiac troponin-T (ab8295) and ranged between ~70-90%.

Gating strategy

FSC/SSC analysis was initially performed to identify individual live cells and exclude cell debris and clusters of two or more cells. Isotype control antibodies were used to determine appropriate gating strategies for myocyte and stromal cell markers. For endogenous reporter-based flow cytometry (ALPK3-tdTomato), the parental hPSC line which does not contain the tdTomato fluorescent reporter was used for gating.

- Tick this box to confirm that a figure exemplifying the gating strategy is provided in the Supplementary Information.